The phloem unloading and sucrose-sequestration pathway in the internodal stem tissue of the *Saccharum* hybrid var. NCo376

Thesis submitted in fulfilment of the

requirements for the degree of

Master of Science

of

Rhodes University

by

Jacqués Gerber

December 2000

The phloem unloading and sucrose-sequestration pathway in the internodal stem tissue of the *Saccharum* hybrid var. NCo376

Internodes 5-8, 10, 13 and 15 of *Saccharum sp.* var. NCo376 were examined for evidence of symplasmic phloem unloading of sucrose from the phloem, via the bundle sheath to the storage parenchyma. The vascular bundle possesses well-isolated phloem comprised of large diameter sieve elements and small diameter companion cells. A layer of phloem parenchyma surrounds the phloem, except where the phloem abuts the crushed protophloem. Outside this is a sclerenchymatous sheath, directly endarch to a parenchymatous bundle sheath, which is surrounded by storage parenchyma. The bundle sheath is interrupted at the centrifugal pole of the vascular bundle by a phloem fibre cap. Scanning Electron Microscopy revealed plasmodesmal fields throughout the bundle sheath and pith tissue. Transmission Electron Microscopy studies provided evidence of plasmodesmal occlusion, but not in all tissues. Aniline blue reactions under UV light indicate the presence of occluded plasmodesmal fields at the phloem parenchyma / sclerenchymatous sheath interface, and in localised regions of cells which are smaller than the surrounding storage parenchyma cells. This suggests a symplasmic transport pathway at these locations, and, based on these positive aniline blue reactions, with regulation via callose-mediated transplasmodesmal transport. Osmotic stress experiments, which included the addition of Ca^{2+}, did not reveal further callose occlusion in the parenchyma, suggesting that the plasmodesmata in these regions may be closed via a noncallosic mechanism. Dye-coupling studies, using Lucifer Yellow (LYCH), which was iontophoretically injected following turgor-pressure equalisation, showed only rare, limited symplastic transport, usually only between the injected

cell and one adjacent cell. Most injections did not result in transport of LYCH, suggesting either a lack of plasmodesmal connectivity, occlusion, or gating of any plasmodesmata present. This limited symplasmic transport, combined with the presence of occluded plasmodesmata at the phloem parenchyma / sclerenchymatous sheath interface suggests the presence of a two-domain phloem-unloading pathway. While symplastic transport may occur from the phloem to the sclerenchymatous sheath, further sucrose transport to the storage parenchyma appears to proceed apoplasmically from the sclerenchymatous sheath / bundle sheath interface, and into storage parenchyma cells across the cell wall and cell membrane via specialised sucrose transporters.

Table of Contents

List of Abbreviations

BPD	Branched plasmodesmata
BS	Bundle sheath
CC	Companion cell
CPD	Critical point drying
CS	Cross section
ER	Endoplasmic reticulum
EtOH	Ethanol alcohol
FAA	Formyl acetic acid
LS	Longitudinal section
LYCH	Lucifer Yellow
P	Parenchyma
PEG6000	Polyethylenglycol 6000
PP	Protophloem
MES buffer	2-[N-Morpholino]ethanesulfonic acid buffer
ML	Middle lamella
NADP-ME	Nicotinamide adenine dinucleotide phosphate - malic acid
PPar	Phloem parenchyma
PD	Plasmodesmata or plasmodesmal field
PTS	Trisodium 3-hydroxy-5, 8, 10-pyrenetrisulfonate
SASEX	South African Sugar Experimental station
SE	Sieve element
SEM	Scanning electron microscopy
SP	Sieve plate
SS	Sclerenchymatous sheath
TEM	Transmission electron microscopy
TS	Transverse section
UDP-glucose	Uridine diphosphate
UV	Ultraviolet
WPI	World Precision Instruments

List of Figures **Page**

List of Tables **Page**

Acknowledgements

Firstly I must acknowledge and thank my supervisor Professor CEJ. Botha for taking me on as a student, organising NRF funding, and allowing me to use his equipment. I also thank the staff of the Rhodes University Electron Microscopy unit, Mr. RHM Cross, Ms Shirley Pinchuck, and Mr. Marvin Randall for their help, advice, and especially for sectioning my blocks for TEM. I wish to thank SASEX for generous funding in the first year of this project, for the provision of setts, and for assistance in understanding the growing process of sugarcane. I single out Derek Watt and Dr Barbara Huckett especially for their assistance. I thank the NRF for funding me, via the studentship organised by Professor CEJ. Botha, from 1998 to 1999. I thank Botany department technicians Mr Eric Tasmer for organising the equipment needed to grow the sugarcane, and Mr Jay Narsai for helping me with the production of light microscopy slides, as well as INVASS, whose growth tunnel I partly filled with sugarcane. I wish to thank Mr Brad Ripley of the Rhodes Botany department for answering the many physiological questions I had. I also thank Mr Bernd Sonnenberg for inspiring me and acting as a sounding board for some of my ideas.

I wish to also thank the following persons for general support and inspiration: Phill (Sididis) Heimann, Kirsty Cordell, Christopher LaRose, Richard James (Smurf) Roberts, Inge von Senger, Julian Puttergill, Marcelle Puttergill, and lastly, but certainly not least, David Hart of Stevenage.

Finally I wish to thank Chloe (Herring) Hardy, the love of my life, without whom I am nothing.

Introduction

1.1 Introduction to *Saccharum* sp. var. NCo376

Saccharum is an NADP-Malic C4 genus within the *Poaceae* (subfamily *Panicoideae*, supertribe *Andropogonanae*, tribe *Andropogonaneae*) (Hattersley 1986). There are six *Saccharum* species, but most sugarcane under cultivation is a hybrid of *S. officinarum* L. This species, and cultivars thereof, is referred to as a "Noble Cane" due to the thickness of the stems (Purseglove 1979 p215). The high sugar content of *Saccharum* is believed to be due to evolutionary pressure, and not due to human intervention (Bull and Glasziou 1963). *Saccharum sp*. var. NCo376 (hereafter referred to as NCo376) is a hybrid derived primarily from *S. officinarum*, but also from *S. spontaneum* and *S. barberi*. Due to its high susceptibility to the sugarcane mosaic virus, and its lower yield compared to newer varieties, it is gradually being phased out, but it still widely grown (Huckett and Botha 1995).

1.1.2 Cultivation of Saccharum sp.

Saccharum is cultivated under field conditions in South Africa (1998/1999 - 427 646 hectares, Pers. com. Watt 2000) for the production of granular sugar and for chewing. Chewing cane is cultivated on a small scale by small farmers. The majority of sugarcane production is for crystallised sucrose, which is used as a sweetener and energy source. The cultivation technique is the same for both. Shallow furrows are dug, either by hand or mechanically, approximately 1.6 m apart, and from 15 to 45 cm deep. The setts are laid in the bottom of the furrows and covered with up to 10 cm of soil. The furrow is gradually filled in with soil.

The setts are laid with the buds in a horizontal plane. Tillers are produced by the bud, and in South Africa are harvested after two years. This first crop is called the "plant crop". The canes are cut back to ground level during harvest. Further tillers are then produced as a ratoon crop. Several ratoon crops may be harvested before the sucrose content of the cane falls below economically viable levels. This fall-off is due to the weaker root production of the ratoon crop as compared with the initial plant crop.

1.1.3 Gross morphology of Saccharum sp. in general, and Saccharum Var. NCo376 in particular.

The primary morphological character of interest is the stem and the attachment of the leaves. The stem is typically between 2.5 and 6 m in length, and only branches at the base where tillers are formed. The stem is solid and is divided into nodes and internodes that are from 1.5 to 6 cm in diameter. The internodes are longest in the middle of the culm, and shortest at the base and apex, are circular to slightly oval in cross-section and generally cylindrical in shape. The stems of NCo376 are covered in a thin layer of wax. Each node has a bud and two rows of root primordia. The leaves are borne in two rows on either side of the stem, and are alternately attached at the nodes. Each cane possesses approximately 10 green, mature leaves at any time, and older leaves dry out as new leaves are formed. The tubular leaf-sheaths surround the culm, and are covered in hairs on the outer surface. NCo376 is free-trashing in that the leaf-sheaths become loose as the leaves dry, eventually allowing the leaves to fall off.

1.1.4 Anatomy of Saccharum sp.

Saccharum displays several typical monocotyledonous features. The vascular bundles are collateral. A peripheral ring of small vascular bundles occurs below the rind, surrounding the ground meristem. Within this, larger vascular bundles are organised spirally. The phloem in the peripheral bundles is greatly reduced (Artschwager 1925), and they are stated sometimes to lack phloem entirely (Jacobsen *et al.* 1992). The larger vascular bundles centripetal to the outermost ring usually have two large xylem vessels. Some phloem parenchyma occurs in association with the phloem, but below the bundle sheath. Protoxylem is usually crushed and occurs at the outer limit of the metaphloem elements. A protoxylem lacuna may not always be present in *Saccharum* vascular bundles (Artschwager 1925). The peripheral vascular bundles, including those with the heavy sclerenchymatous caps at the xylem poles are apparently non-functional in long distance transport. Instead they are thought to fulfil a supportive function (Walsh *et al.* 1996). Hartt *et al.* 1962 confirmed this by demonstrating that radiolabled sucrose (supplied to the plant as $C^{14}O_2$) is translocated only via the pith vascular bundles. The pith vascular bundles are associated with a sclerenchymatous bundle sheath, and the region of sclerotisation becomes larger in the more peripherally-located bundles, where the parenchymatous tissues at the xylem pole become progressively sclerotised (Artschwager 1925). In internodes near the base of the plant, these parenchyma cells usually become completely sclerenchymatous, with the exception of isolated storage parenchyma cells (Jacobsen *et al.* 1992). Vascular bundles in the pith usually have a prominent protoxylem lacuna (Artschwager 1925).

1.2 Metabolism of sucrose as related to sequestration

Welbaum and Meinzer (1990) demonstrated that the osmotic potential of apoplasmic sucrose might exceed -2.2 MPa. Glasziou (1960a) and Glasziou and Gayler (1972) claimed that sucrose sequestration occurs from the apoplasm to the cell inner space (cytoplasm and/or vacuole - not specified in article). This involves the lysis of sucrose to glucose and fructose. Sucrose is hydrolysed by an extracellular invertase before being taken up (Komor *et al.* 1981). The reduced hexoses are then transported across the cell wall into the cell cytoplasm. Recombination to form sucrose occurs in the cytoplasm (Glasziou 1960a, Glasziou 1960b, Glasziou and Gayler 1972). The rates for sucrose and glucose uptake in young tissues are 6 and 15 times higher respectively, than for mature tissues. Sugar phosphates begin to appear in cell extracts of sugarcane cells in suspension culture bathed in ^{14}C labelled glucose after 5 seconds, while fructose and sucrose appear after 15 and 30 seconds respectively. The relative proportions of glucose, fructose and sucrose in immature tissues are different from the tissues leaking into the medium, indicating that immature tissues are 8-10 times more permeable to reducing sugars (fructose and glucose) than to sucrose. This rate is not closely correlated with tissue sugar content. The rate of uptake decreases initially, and then increases with increasing maturity. Changes in the rate of leaking indicate the presence of more than one sucrose pool within the tissue (Glasziou 1960a). There is no detectable uptake of sucrose from the medium (Maretski and Thom 1972). However, tracer studies have demonstrated that the inner-space fructose and glucose are derived from the inversion of inner space sucrose. Changes in

the sucrose concentration of the medium have no effect on the ratio of sucrose to glucose and fructose. A turnover time of 8.6 h was found for the sucrose pool, and from 31-46 h for the glucose/fructose pool. Maturation is marked by an increase in the sucrose content, and a decrease in the glucose and fructose content (Glasziou 1960b, Whittaker and Botha 1997). If the inversion of sucrose forms an important factor in the storage of sucrose, then the rate of sucrose inversion must decline with maturation (Glasziou 1960b). The capacity of cells to take up hexoses from outside the cell exceeds observed rates of sucrose sequestration. On this basis, Komor *et al.* (1981) concluded that the sequestration pathway is apoplasmic.

Peaks in the sucrose accumulation rate correspond with the doubling of the initial sucrose phosphate synthase activity. Sucrose synthase activity, in the synthesis direction, peaks during the maximal sucrose accumulation, and is lower and decreases during the culture cycle in the hydrolysis direction (Goldner *et al.* 1991). Invertase follows a similar pattern to the hydrolysis direction. Acid invertase has been shown to have a high initial rate of activity, followed by a rapid decline more especially during sucrose accumulation. Sucrose synthesis is suggested to be due to sucrose phosphate synthase activity (Glasziou and Gayler 1972, Goldner *et al.* 1991), with sucrose synthase activity functioning in a degradation capacity (Goldner *et al.* 1991). The elongation of sugarcane internodes is directly correlated with the activity of acid invertase (Hatch and Glasziou 1963a, Slack 1965). Veith and Komor (1993) did concur however. The rates of enzymes involved in sucrose metabolism are

more related to the growth rate than to the rate of sucrose sequestration (Veith and Komor 1993). Soluble acid invertase does not occur in mature storage tissue. A neutral invertase is however present (Hatch and Glasziou 1963a).

Replacement of the 1'-hydroxyl of sucrose by fluorine reduces the hydrolysis of 1'-fluorosucrose to 2 % of that of sucrose, but does not reduce recognition, binding or transport by a sucrose carrier. Both sugars are recognised at the same binding site at the plasmalemma, but that the sucrose carrier has a higher affinity for 1'-fluorosucrose that for sucrose (Thom and Maretski 1992, Hitz *et al.* 1985). Kinetics indicates that membrane passage and substrate release to the protoplast interior are rate limiting to transport. Recognition of sucrose at the inner membrane of the sucrose transport protein appears to be different to the recognition and binding at the external surface. 1'-fluorosucrose is absorbed slowly by corn root segments, due to the need for sucrose hydrolysis by cell wall invertase prior to active uptake (Hitz *et al.* 1985).

There is no evidence for a proton/sucrose antiport system similar to that reported in sugarbeet. The ratio of sucrose uptake to proton transport (as % fluorescence quench/mg protein) was found to be 1:13, compared with 1:62 in sugarbeet. The difference is due to higher transport rates in sugarcane and differences in protein transport (Williams *et al.* 1990).

1.2.2 Sucrose accumulation in sugarcane

The primary photosynthate in sugarcane is sucrose. Hatch and Glasziou (1963b) suggest that this is translocated intact from the leaves to the stems, and that glucose and fructose can enter the translocation stream, but are converted en-route to sucrose. Bowen and Hunter (1972) demonstrate that sucrose is hydrolysed prior to uptake from the apoplasm. There is an apparent physiological limit to sugar accumulation within *Saccharum* at 27 % of fresh weight (Bull and Glasziou 1963). Sugar uptake by sliced sugarcane has been shown to occur in two stages. The initial uptake takes place within one hour, and results in a sugar concentration that is proportional to the external concentration. This sugar can be washed away, indicating that it exists in the free space. However, secondary uptake may continue for up to 60 h, against a 200-fold concentration gradient. This sugar does not diffuse out when the slices are washed, indicating that the sugar is taken up into the cell cytoplasm and/or vacuole. This has been suggested to be an active accumulation process (Bieleski 1960). The accumulation rates for sucrose, glucose and fructose are a hyperbolic function of the sugar concentration, suggesting the presence of a sugar carrier. Glucose (11 m*M*) and sucrose (5.8 m*M*) interact competitively, indicating a common carrier, with glucose inhibiting sucrose uptake (relative accumulation rate = 0.35) to a greater degree than the inverse (relative accumulation rate = 0.90). All sugars appear primarily as sucrose in the cell inner space (cytoplasm and/or vacuole - not specified in article) (Bieleski 1962). Apoplasmic sucrose has a similar concentration, approximately 20 %, to that of vacuolar sucrose. This suggests that the main path of sugar transfer and

accumulation is apoplasmic (Hawker 1965). It has been shown that mature tissues do not accumulate sucrose (Bieleski 1960). Komor (1994) regards all internodes above internode 12 (counting from first visible leaf = Internode 7 counting from first enlarged internode) as mature.

1.3 Phloem unloading and storage tissue loading.

According to Oparka (1990) phloem unloading is the process whereby photosynthates are transported from the phloem tissue to surrounding tissues where it is either sequestrated or utilised. The photosynthetic end-product in sugarcane is sucrose. Sucrose is transported from the leaves via the sieve elements (SE). The true phloem-unloading step is from the sieve elements to the companion cells (CC) (Oparka, 1990). The SE-CC complex is connected by abundant plasmodesmata, and is essentially a functional unit (Oparka 1990). There are two possible pathways for the movement of photoassimilates. This may be symplasmically into the vascular parenchyma via plasmodesmata, or apoplasmically direct across the plasmalemma and into the apoplasm. Although symplasmic isolation of the SE-CC complex has been reported for minor veins in leaves (see Botha and Cross 1997, and literature cited), this has not been reported for SE-CC complexes in sink tissue (Oparka 1990). Sink cells are known to possess the ability to accumulate solutes from the apoplasm (Bieleski 1960, Oparka 1990). Patrick (1990) suggests that phloem unloading may be regulated by a turgor mediated-feedback loop, which controls plasmodesmata along the symplasmic pathway in sink tissues, such as in *Abutilon sp*. nectaries (Gunning and Hughes 1976) and potato tubers (Oparka and Prior 1988). Hayes

et al. (1987) suggest that phloem unloading in *Phaseolus vulgaris* follows a symplasmic route in summer-grown plants, and an apoplasmic route in winter-grown plants. They observed that chloromercuribenzene sulphonic acid blocked the uptake of sucrose being loaded into the storage cells in the stem, but did not effect the pool size of sugars in the apoplasm. Aloni *et al.* (1986) examined the efflux characteristics of ^{14}C-labelled sugars in excised segments of *Vicia faba* stems. They concluded, on the basis that cleavage of unloaded sucrose (via intracellular invertase or cell wall acid invertase) is only apparent after several h, that the phloem unloading pathway is apoplasmic, and that a membrane bound carrier may be involved in sucrose translocation. Oparka and Wright (1988) found that the total uptake of [^{14}C] sucrose in potato tuber discs was strongly correlated with both turgor potential and osmotic potential when the discs were bathed in mannitol solutions with a concentration of between 100 m*M* and 300 m*M*. Sucrose uptake and its conversion to starch improved at 300 m*M* mannitol, which the authors suggest is indicative of a turgor effect rather than an osmotic effect. Increased sucrose uptake at mannitol concentrations exceeding 400 m*M* results from uptake into the apoplasmic space. Cosgrove and Cleland (1983), working on pea stems, as well as Hawker (1965), and Glasziou and Gayler (1972), working on sugarcane, suggest that strong sinks ie storage cells, are characterised by high concentrations of osmotically active solutes in the apoplasm. Eschrich (1980, cited by Wolswinkel 1985) suggested that the osmotic potential of the apoplasm might be lowered by free space acid invertase activity hydrolysing sucrose into hexoses. Oparka and Prior (1988) showed that plasmolysis of storage tissues prevents the transport of

[^{14}C]sucrose in the potato, and they suggest on this basis that at least part of the transport pathway from the phloem to the storage parenchyma is symplasmic. The storage cells of the potato tuber are connected to one another by many plasmodesmata (Oparka and Prior, 1988), and also from the storage parenchyma to the transport phloem (Oparka 1986). Oparka and Prior (1988) concluded that the transport pathway in the potato tuber is probably primarily symplasmic. Chapleo and Hall (1988) concluded that the sucrose unloading pathway into the root cortex of *Ricinus communis* L. is symplasmic, and that this precludes a direct role for an apoplasmic invertase in sucrose transport. *Ricinus* seedlings were exposed to $^{14}CO_2$ for 1 h, the roots bathed to extract apoplasmic sucrose and hexoses, and the amount of ^{14}C compounds, including sucrose, in the bathing medium was determined. ^{14}C sucrose amounted to approximately 1.27 % of the extracted soluble ^{14}C compounds. They suggest that the initial translocated sucrose metabolic step be either via acid invertase in the vacuole, or sucrose synthase in the cytoplasm. Schmalstig and Geiger (1985) found that passively transported xenobiotic sugars imported via the phloem by sink leaves of *Beta vulgaris*, was evenly distributed throughout the leaf, while by contrast, sugar supplied to the apoplasm via the petiole was confined to the vicinity of the major veins. This indicates that the sugar was transported from the phloem to the mesophyll via the symplasm.

1.3.2 Plasmodesmata in phloem unloading and storage cell loading.

Ding *et al.* (1992) describe plasmodesmata as having a plasma membrane which is continuous through the plasmodesmal pore between adjacent cells,

with an axial desmotubule which runs through the pore and is connected to or continuous with the endoplasmic reticulum. The ends of the plasmodesma are constricted at the neck region. Lucas *et al.* (1993) state that the desmotubule (also referred to as the appressed endoplasmic reticulum) forms a continuous region of endoplasmic reticulum between cells. The desmotubule may have a central rod at the centre (Botha and Cross 2000). The outer leaflet of the plasmamembrane may be composed of granular subunits, while the inner plasmamembrane leaflet is attached to the outer wall of the desmotubule by "thread-like spokes" (Botha and Cross 2000). Welbaum *et al.* (1992) examined the distribution of plasmodesmata in sugarcane (*Saccharum sp*. hybrid, cultivar H65-7052). They examined the tenth internode below the top visible dewlap. Plasmodesma were observed between adjacent sclerenchymatous-sheath cells, between sclerenchymatous-sheath and phloem companion cells, and between sclerenchymatous-sheath and adjacent storage parenchyma cells. They observed that the plasmodesmata traverse the suberin lamella in the sclerenchymatous sheath, opening a potential symplasmic pathway. No examination of plasmodesmal functionality or density was made. As mentioned earlier, they concluded from morphological evidence that the apoplasm in sugarcane is segregated into two separate spaces, one within the vascular bundle and the other being the storage tissue. Using the apoplasmically-confined cell wall-binding fluorescent dye Cellufluor, they found that there was no fluorescence outside the cell walls of the protoxylem and metaxylem. They suggested that a semi-permeable barrier exists between the xylem and the storage parenchyma which restricts the movement of large molecular weight

solutes, but permits the movement of water (Welbaum *et al.* 1992). Giaquinta *et al.* (1983) demonstrated that asymmetrically labelled [^{14}C](fructosyl)sucrose remains intact when translocated in germinating *Zea mays* seeds to the roots, indicating that it does not undergo hydrolysis in the apoplasm. Exogenous sucrose is hydrolysed by a cell wall invertase prior to uptake in *Z. mays* root cortical cells. This indicates that the asymmetrically labelled [^{14}C](fructosyl)sucrose is unloaded symplasmically into the root cortical cells. Similarly, Dick and ap Rees (1974) found that asymmetry of [^{14}C]glucosyl sucrose was retained in root cortical tissues of *Pisum sativum*. Wyse (1979), working on sugar beet root tissue using asymmetrically labelled sucrose([^{14}C]glucose), observed that 80 % asymmetry was retained, indicating that the sucrose was not hydrolysed during uptake, which was against a concentration gradient and required metabolic energy. He suggests that sucrose transport between the apoplasm and the vacuole occurs via a nonsaturating carrier at locations where the tonoplast and plasmalemma are appressed.

Dye coupling studies of photosynthate sinks, such as avocado fruit (Moore-Gordon *et al.* 1998), revealed a high degree of symplasmic connectivity in normal fruit, with rapid radial movement of Lucifer Yellow into surrounding tissues. In fruit, which had been treated with abcisic acid, this radial movement was greatly retarded. Transmission electron microscope studies of the plasmodesmata showed that the normal fruit had plasmodesmata in which the neck regions were slightly constricted. The mesocarp plasmodesmata of

phenotypically small fruit were occluded with electron dense material. Electron dense material was also deposited outside the necks of the plasmodesmata, thereby gating the plasmodesmata. Botha and Cross (2000) speculate that this electron dense material may be callose (1,3-β-glucan), which is known to occlude plasmodesmal fields following wounding (Hughes and Gunning 1980, Lucas *et al.* 1993). Hayes *et al.* (1987) observed that induced cellular plasmolysis of *Phaseolus vulgaris* with a 1 M mannitol solution appeared to sever plasmodesmal interconnectivity between all stem cells with the exception of the sieve element-companion cell complex. Curiously, they found that storage cell sucrose loading was unaffected by cellular plasmolysis following stem tissue rehydration.

1.3.3 The role of calcium in plasmodesmal regulation via the deposition of callose

In the event of wounding, the plant must be able either to down-regulate the plasmodesmal size exclusion limit or seal off the plasmodesmata of intact cells rapidly, thus preventing the loss of metabolites (Lucas *et al.* 1993). Calcium, in the form of the Ca^{2+} cation, is involved in the regulation and synthesis of 1,3-β-glucan (callose) (Kauss 1987). Callose formation is known to occlude plasmodesmal fields following wounding events involving a loss of turgor pressure (Lucas *et al.* 1993). Callose is synthesised by 1,3-β-glucan synthase, which is activated by local increases in cytoplasmic Ca^{2+}. This activation is reversible, and appears to result from a direct allosteric interaction of Ca^{2+} with 1,3-β-glucan synthase. This activation does not appear to be mediated by

calmodulin (Kauss 1987). Nonetheless Hong *et al.* (1999) identified a calmodulin-regulated Ca^{2+}-ATPase in the endoplasmic reticulum of *Arabidopsis* cv Columbia. Increases in cytoplasmic Ca^{2+} due to wounding may control the degree of plasmodesmal constriction (Kauss 1987). According to Olesen and Robards (1990), the cytoplasmic annulus may become constricted or totally occluded, depending on the degree of callose deposition. Currier and Webster (1964) observed that there was a progressive loss of callose deposited in plasmodesmal pits over eight days following ultrasound stimulation of callose deposition in *Gossypium hirsutum* L., var. Acala. Botha and Cross (2000) observed that the desmotubule appears to be absent from callose occluded plasmodesmata in the storage parenchyma of *Saccharum sp*. var. NCo376, and they suggest that this could be part of the plasmodesmal down-regulation associated with the wounding response. Hughes and Gunning (1980) observed that callose deposition at the plasmodesma could be induced using glutaraldehyde. They concluded that this deposition was an artefact on the basis of controls using freeze-fixation techniques.

1.4 Phloem unloading and storage parenchyma loading in sugarcane

The phloem apoplasm (ie the cell wall and intercellular spaces) of sugarcane is claimed to be isolated from the storage parenchyma apoplasm by a sheath of lignified, suberised fibres. This would preclude the apoplasmic transport of sucrose to the storage parenchyma from the phloem (Jacobsen *et al.* 1992, Walsh *et al.* 1996). The apoplasmic tracer dyes trisodium 3-hydroxy-5, 8,10-pyrenetrisulfonate (PTS) and amido black 10 B are confined to the vascular

bundles above the site of dye introduction, when introduced into the cut ends of the stem, and do not infiltrate the storage parenchyma. This suggests that the transport pathway from the phloem to the storage parenchyma via the bundle sheath is symplasmic (Jacobsen *et al.* 1992). This is in direct contradiction to the findings of Komor *et al.* (1981). Thom and Maretzki (1991) concluded that sugarcane storage tissue can take up intact sucrose in addition to hexoses. They characterise this uptake as "poor" (Thom and Maretzki 1991 p558), and provide support for the symplasmic transport of sucrose from the phloem via the plasmodesma to the storage parenchyma. Welbaum *et al.* (1992), using greenhouse grown plants, concluded that the sclerenchymatous sheath surrounding the vascular bundles divided the sugarcane stalk into two separate compartments. This is on the basis that xylem sap is nearly sucrose free, while the apoplasm outside the sheath contains a high concentration of sucrose. The osmolarity (Ψ) of the storage tissue from internode 10 was measured at -0.8 MPa. Greenhouse-grown sugarcane plants accumulate less sucrose than do field-grown plants (Welbaum *et al.*, 1992, citing Welbaum and Meinzer 1990 unpublished results). These authors noted that apoplasmic dyes are confined to the vascular bundles, and suggest that these fibres are permeable to water, but not to macromolecules such as sucrose. They suggest that phloem unloading in sugarcane requires a symplasmic step within the vascular bundle and across the fibre sheath. However Eastman *et al.* (1988) demonstrate that the suberised bundle sheaths in the stems of C_4/NADP-ME grass species is not only permeable to water, but also to PTS. However Zimmermann and Steudle (1998) demonstrated that the apoplasmic flow of PTS is not prevented by the

suberised exodermis of *Zea mays* roots, while the apoplasmic flow of water is excluded at this point. The apoplasmic flow of PTS is prevented by the suberised endodermis, which does not appear completely to exclude the apoplasmic transport of water. The bundle sheath cells in the leaves of *Zea mays* are also suberised, but only on their outer radial and tangential walls, with a suberin lamella only being present in the inner tangential walls at the sites of plasmodesma (Evert *et al.* 1977). The bundle sheath cells of *Themeda triandra* are likewise suberised, and form a barrier to the movement of solutes from the mesophyll to the bundle sheath. This necessitates the presence of a symplasmic pathway at this juncture in the phloem-loading pathway in the leaves (Botha and Evert 1988). The longitudinal vascular bundles of sugarcane are surrounded by a suberised, chlorenchymatous bundle sheath, as well as a suberised sheath of thick walled mestome sheath cells (Robinson-Beers and Evert 1990). These even intervene between the chlorenchymatous bundle sheath and the large metaxylem vessels, contrary to the usual arrangement in NADP-malic C_4 grasses (Hattersley and Watson 1976, Robinson-Beers and Evert 1990). This is however the normal arrangement in sugarcane (Hattersley and Watson 1976).

1.5 Aims

The principle aims of the research were to examine the sucrose transport and sequestration pathway in *Saccharum sp*. Var. NCo376, by examining the stalk tissue using light and electron microscopy based techniques, coupled with fluorescence microscope studies, to try to determine the relative state of

symplasmic interconnectivity between the vascular tissues and storage parenchyma by examining the assumed functional state of the plasmodesma. In addition, It is hoped that the work presented will be of use in furthering understanding of the pathways and regulation of sucrose sequestration in sugarcane. Hopefully, this will provide baseline information from which modifications could be made to the genetic makeup, and hence the physiology of the crop in order to enhance sugar production.

1.6 Hypotheses

It is not possible to demonstrate apoplasmic transport with the methods employed in this study. Rather, they can be used to demonstrate the presence or absence of symplasmic transport. It is hoped that the sucrose sequestration pathway in NCo376 is apoplasmic, as this is consistent with physiological observations made on sugarcane (Pers. com. Botha FC 1999). With due consideration for the falsifiability of the hypothesis, the techniques used in this thesis can be used to test the null hypothesis by attempting to demonstrate the presence of a symplasmic pathway. If the absence of symplasmic transport is a general characteristic, it can be inferred that the transport pathway is apoplasmic.

Null Hypothesis: The post-phloem unloading and sucrose sequestration pathway in *Saccharum* var. NCo376 is symplasmic.

Alternate Hypothesis: The post-phloem unloading and sucrose sequestration pathway in *Saccharum* var. NCo376 is not symplasmic.

Materials and Methods

2.1 Plant material and preparation

Setts of the *Saccharum* hybrid var. NCo376 were harvested from plants grown from setts provided by SASEX (Mount Edgecombe, KwaZulu-Natal, South Africa). The setts were planted in potting containers cut from 210 L drums. 30 eight-mm drainage holes were drilled in the bottom. Any drums not already lined with an epoxy layer were painted inside with iron oxide primer to inhibit rust formation. All drums were placed on bricks to assist drainage. An approximately 5 cm thick layer of gravel was placed in the bottom of each drum for drainage. The drums was then filled with a mixture of builders' sand and topsoil, in approximately equal proportions. Ten pots were planted in January 1998. Five of these were placed in a greenhouse, and the remainder placed outside, on the north face of the greenhouse for maximum insolation. These ten drums were fertilised with approximately two handfuls of NPK 2-3-2 (N 63 g/kg, P 96 g/kg, K 63 g/kg + Zn 5 g/kg) (Kynoch, South Africa). The drums in the greenhouse were planted with setts, while plants planted earlier in March 1997 were transplanted into the outside drums. All drums were subsequently moved into a growth tunnel in September 1998 (see Fig. 1A). Ten additional half-drums were planted with setts in the tunnel in October 1998, of which only five produced tillers. These drums were initially fertilised with urea using one handful per drum. The initial tested soil pH was 5.2, and was counteracted by the addition of dolomitic lime at a rate of two handfuls per pot to bring the pH to approximately 6.9. This acidity was caused by nitrogen fertilisation. 5 mL (A medicine spoon of 5 mL capacity was used) pure sulfur was also added following a consultation with

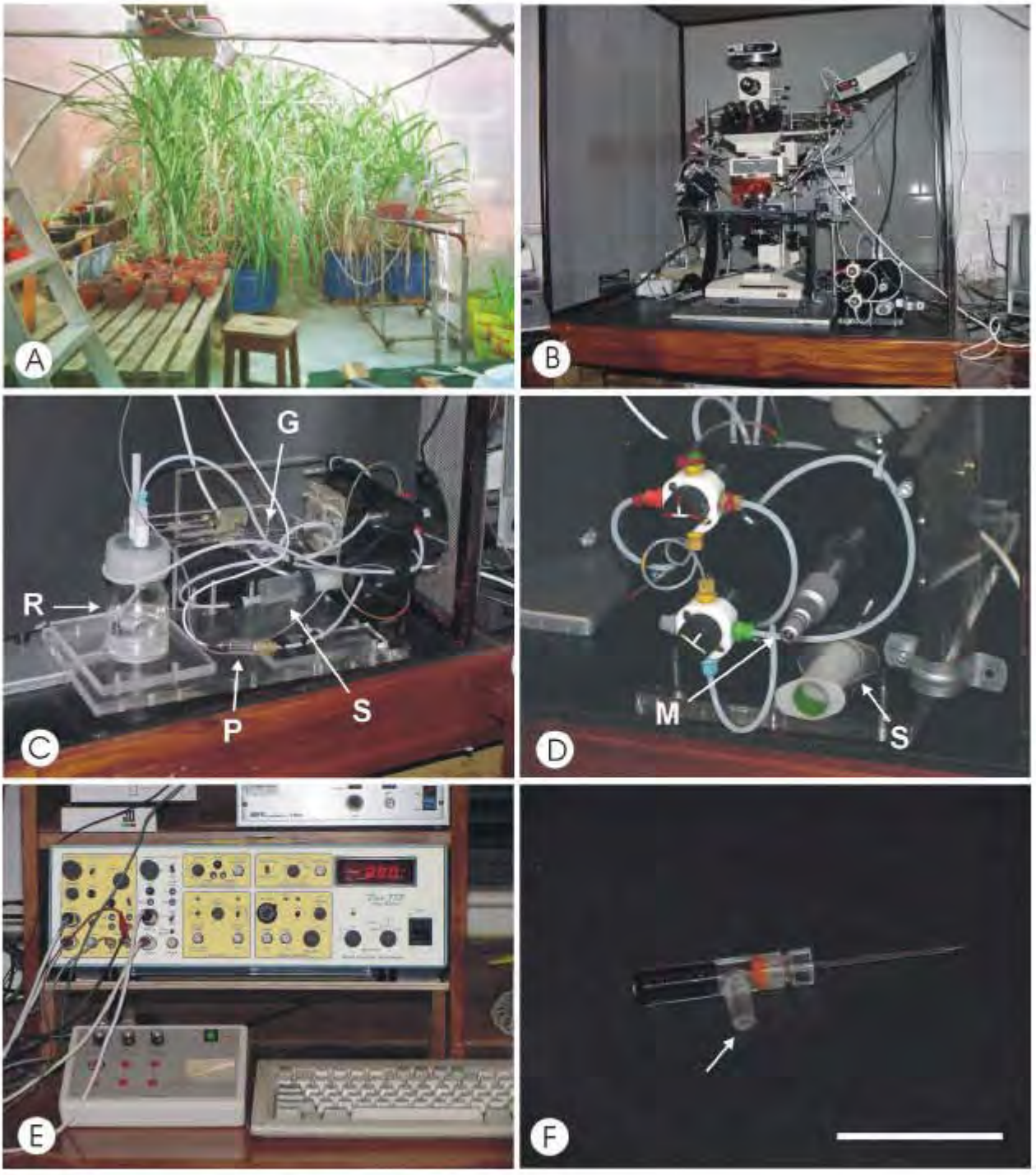
A
B
G
R
P
S
C
M
S
D
E
F

Fig. 1: Detail showing sugarcane growth and equipment used in pressure-assisted microiontophoresis. (**A**) Sugarcane planted in $^{1}/_{2}$ drums in the growth-tunnel. Older plants are in the middle of the tunnel, and younger plants towards the right hand side. (**B**) Shows the Olympus BH-1 microscope set up for pressure-assisted microiontophoresis in a Faraday cage. (**C**) The pressure injector from rear left side showing the arrangement of the pressure sensor (P), silicon oil reservoir (R), filling syringe (S) and micrometer driven gas-chromatography syringe (G). (**D**) Detail of the pressure injector front face showing valves, driving micrometer (M) and filling syringe (S). (**E**) The WPI Duo-773 electrometer and PM10 Piezo controller used for microinjection. (**F**) Shows a WPI microelectrode holder with Ag/AgCl half-cell and side entry port (arrow) for pressure, and microelectrode assembly. (F) Bar = 30 mm

the Agronomy department at SASEX. Plants were watered whenever the soil surface appeared dry, on average once every three days, but at least once per day during midsummer, Water was permitted to pool to a depth of between two and three cm in each drum. The five drums originally planted in October 1998, which did not show any shooting were replanted in February 1999. The unsprouted setts were removed, and one 30 dm3 bag of Ideal Compost (Coastal Livestock Farming cc, Coega, South Africa) (25 g/kg N, 13 g/kg P, 6 g/kg K, 26 g/kg Ca, 5 g/kg Mg, 4 g/kg Fe, 1 g/kg Cu, 1 g/kg Zn: pH 5.8) was added to the original soil/sand mixture. This was mixed thoroughly, and new setts planted.

2.2 Anatomical Studies

2.2.1 Light microscopy

Transverse and longitudinal sections were cut from segments of internodes 5-8, 10, 13 and 15, and placed in vials containing formyl acetic acid (FAA) for one week, with three changes, to ensure fixation. They were then dehydrated in an ethanol and normal butyl alcohol series (Table 1).

The segments were then infiltrated over a period of one week with paraplast wax in an embedding oven at 60^{o}C, after which the segments were blocked and sectioned at 15 μm using a Leitz Wetzlar (Germany) rotary microtome. Sections were then picked up onto slides. Due to the size of the sections typically 2 cm long, only one section was picked up per slide.

Table 1: Duration and composition of dehydration alcohol series for light microscopy embedding.

Time, h	Alcohol mixture, %
48	50 EtOH
48	70 EtOH
48	35 butyl-alcohol
48	55 butyl-alcohol
48	75 butyl-alcohol
24	100 butyl-alcohol
24	100 butyl-alcohol
24	100 butyl-alcohol

These were then de-waxed in 3 changes of xylol, stained in Safranin and Fast Green, and mounted under standard coverslips (Superior, West Germany) using Canada Balsam. Mounted slides were cured at 37^{o}C for 1 week in an embedding oven. Selected sections were photographed on an Olympus BX50 microscope equipped with an Olympus PM-30 + PM-C35DX camera system (Olympus, Japan), an Olympus PE 3.3X camera eyepiece, and a UPlanfluor 40X objective with a 0.75 numerical aperture, using Fujicolor Superia 100 ASA colour negative film.

2.2.2 Scanning electron microscopy

Radial sections approximately 5 mm thick were cut from the middle of internodes 5-8, 10, 13 and 15. A 5 mm thick slice was cut to include the inner and outer pith, but excluding the rind. This was then cut into blocks approximately 5 mm^3,and quickly frozen in nitrogen slush, after which the segments were fractured with a clean single-edged razor blade (ASR, U.S.A.) under liquid nitrogen. The still frozen segments were placed glass vials

containing 2.5 % glutaraldehyde in 0.1 M phosphate buffer and fixed overnight in the refrigerator (6^{o}C). The phosphate buffer was then decanted, and the tissue dehydrated in a graded ethanol series (30 %, 50 %, 70 %, 80 %, 90 %, 2 X 100 %), each stage lasting 15 min. The tissue was brought up to room temperature after the 80 % ETOH change. The final ethanol was replaced with 75:25 ETOH : amyl acetate, and allowed to infiltrate for 20 min. This was repeated with 50:50 and 25:75 ethanol : amyl acetate, and 100 % amyl acetate. The samples were placed in CPD baskets under 100 % amyl acetate in a CPD boat and critical point dried in a Polaron E3000-049 Critical Point Drier (Polaron Equipment, Inc., Hatfield, Pa., USA). The samples were then attached to brass stubs with graphite tape (SPI Supplies, Structure Probe, Inc. West Chester, USA), ensuring that at least one tissue piece was aligned for TS, and gold coated in an E5100 SEM Coating Unit (BioRad, Polaron Division: Polaron Equipment, Inc., Hatfield, Philadelphia, USA) equipped with an E5500 Film Thickness Monitor (BioRad, Polaron Division: Polaron Equipment, Inc., Hatfield, Philadelphia, USA). The samples were examined in a JEOL JSM 840 Scanning Electron Microscope (JEOL, Tokyo, Japan), and areas of interest photographed on Agfapan ISO 100/21 film (Agfa-Gevart AG, Germany). Initial studies used variable magnification with respect to the image of interest. In order to simplify subsequent identification of tissues, low power (70X) and intermediate magnification (130X) images were made, from which individual cells in each localised area were photographed at 1000X magnification to show the distribution of plasmodesmal fields. These images were taken at 12.5 kV, and higher magnification images were taken of individual plasmodesmal fields at

22.5 kV to show details of plasmodesmal pit fields. Where possible, pit depths were measured on some images with a digital calliper, using the magnification bar printed in the micrograph as a reference

2.3 Transmission electron microscopy

Radial sections approximately 3 mm thick were cut from the middle of internodes 5-8, 10, 13 and 15 with a single edged razor blade. These were diced under cold (6^{o}C) 0.5 M sodium cacodylate buffer containing 0.6 M mannitol, producing pieces 1 mm X 1 mm X 2 mm in size. These blocks transferred using a small artist's brush to glass vials containing 6 % glutaraldehyde in sodium cacodylate buffer. 0.05 M sodium cacodylate buffer was initially used, but it was found that this osmolarity was too low for adequate infiltration with sugarcane stem tissue, and 0.5 M sodium cacodylate buffer was substituted. The fixative was changed after twenty min, the vials placed in a vacuum desiccator, and carefully subjected to a 17 kPa vacuum. The vacuum was released slowly after one h. The fixative was changed, the stoppers replaced, and the vials placed in the refrigerator to fix for a further eight h. The fixative was changed twice during this period. The tissue was then washed in 4 changes of 0.5 M sodium cacodylate buffer, each of 20 min duration. The tissue was then transferred to 2 % osmium tetroxide in 0.5 M sodium cacodylate buffer, and kept in the refrigerator overnight. The tissue was then washed in 4 changes of 0.5 M buffer, each of 20 min duration, to remove all traces of unbound osmium tetroxide. The vials were returned to the refrigerator after each change. The buffer was then decanted off, and the tissue dehydrated in a

graded ethanol series from 10 % to 90 %, each stage lasting 20 min. The tissue was allowed to come up to room temperature after the 80 % change. The tissue was then placed in 100 % EtOH for 40 min with three changes. This was followed with 30 min in EtOH : propylene oxide (1:1 v/v), followed by 3 changes of 100 % propylene oxide, each of approximately 25 min duration. Hard setting low viscosity Spurr's resin (Spurr 1969) was used. The tissue was processed through three changes of resin : propylene oxide (1:3 v/v for 3 h, 1:1 v/v for 24 h, 3:1 v/v for 24 h), followed by 24 h in 100 % resin. Small wads of absorbent tissue paper were inserted into the vials under the surface of the resin to prevent contact between the tissue and the atmosphere. The wadding was changed at every resin change. The tissue was left under a vacuum of approximately 17 kPa for 2 h at the 3:1 stage. The tissue was then placed in fresh resin in new rubber moulds, and polymerised for 15 h at 60^{o}C. Monitor sections were cut on a RMC MT-7 Ultramicrotome (Research and Manufacturing Co., Inc., Tucson, Arizona, USA) with a glass knife, stained in for one minute in toluidine blue, rinsed in distilled water, and mounted for light microscopy under glass coverslips (Superior, West Germany) with Depex mounting medium (G. T. Gurr, London, England).

2.3.1 Preparation of sections and examination

Sections for TEM were cut using a LKB 8800 Ultramicrotome (Bromma, Stockholm, Sweden), using a diamond knife (Drukker, Netherlands). All sections were mounted on 300 mesh copper grids (SPI Suppliers, Philadelphia, USA) and stained for 30 min in uranyl acetate followed by five min in lead

citrate. Each staining stage was followed by two gentle washes of distilled water, after which the grids were dried on filter paper. The sections were then examined in a JEOL JSM 1210 transmission electron microscope (JEOL, Tokyo, Japan) at 100 kV. Micrographs were taken of plasmodesmal fields in the storage parenchyma and bundle sheaths.

2.4 Preparation of tissue for examination of callose using aniline blue fluorescence

Radial stem segments of internodes 5-8, 10, 13 and 15 were cut using ASR single-edged razor blades. These were placed in baths of mannitol osmotica for approximately 1 h. Four mannitol treatments were used:

1. 0.4 M mannitol (7.288 g mannitol in 100 mL dH_20)
2. 0.4 M mannitol + 50 m*M* Ca^{2+} (7.288 g mannitol + 1.182 g $Ca(NO_3)_2.4H_2O$ in 100 mL dH_20)
3. 0.9 M mannitol (16.386 g mannitol in 100 mL dH_20)
4. 0.9 M mannitol + 50 m*M* Ca^{2+} (16.386 g mannitol + 1.182 g $Ca(NO_3)_2.4H_2O$ in 100 mL dH_20)

(Pers. com. Botha 1999) (Ca^{2+} source: $Ca(NO_3)_2.4H_2O$) (Associated Chemical Enterprises c.c., Reuvan, South Africa). These were trimmed to remove the rind, and longitudinally sectioned under the buffer surface with a halved double-sided razor blade. Controls were made using tissue that was sectioned under tap water immediately after being cut from stem segments. Sections were then transferred to glass slides and stained with 0.5 % (w/v) aniline blue WS (G T Gurr, London, England) in the appropriate buffer solution. The aniline blue was

dissolved in distilled water for the control. These were immediately examined for the presence of callose, and photographed on a Zeiss Junior microscope using a Plan-neofluar 25 X oil / glycerine / water immersion objective lens with a 1.0 NA, and a 50 W high-pressure mercury UV lamp. The sections were photographed using a Zeiss MC63 + M35 camera system (Germany) with Fujichrome Provia 400 slide film. The filter sets used were BP: 425-440, FT: 475, LP: 460 (Chroma Technology Corp, Battleboro, U.S.A.), and BP: 450-490, FT 510, LP: 460 (Zeiss, Germany).

After exposure, the slide film was developed by Colour 2000 (Port Elizabeth, South Africa). Selected slides were scanned using a Nikon LS-1000 35 mm Film Scanner (NikonUK, Kingston, Surrey, UK) at 600-1200 pixels per inch resolution, and saved as tagged information format (TIF) files. The digital images were imported into CorelDraw 9, and adjusted if necessary using the Hue-Saturation-Lightness (Hue: 42, Saturation: -53, Lightness: -64) and Brightness-Contrast-Intensity (Brightness: -6, Contrast: 58, Intensity: -6) tools

2.5 Pressure-assisted microiontophoresis

Fresh plants were harvested for each experiment. Individual internodes, specifically internodes 5-8, 10,13 and 15, were isolated. These were sectioned longitudinally using new ASR single-edged razor blades, which had been modified by removing the aluminium safety backing (the projection had been found to macerate the surface of the sections as they were cut) Sections were approximately 1 mm thick. Sectioning was done in cold MES buffer solution (10

m*M* NaOH-MES) (Sigma-Aldrich, Germany) (Elabtec c.c., Port Elizabeth, South Africa) with added 0.5 m*M* KCl, $MgCl_2$ and $CaCl_2$ in 125 m*M* mannitol (Sigma-Aldrich, Germany) (Elabtec c.c., Port Elizabeth, South Africa). Polyethylenglycol 6000 (PEG 6000) (Merck-Schuchardt. Germany) was added to the MES buffer solution to counteract the high osmolarity of the sucrose solute in the injected cells. 25 g of PEG 6000 was added to 100 mL buffer to give the MES buffer an osmolarity of -1060 kPa. This was found to be too high for internodes 5 and 6, causing spontaneous injections when the cell wall was pierced, and resulting in leaking after the needle was withdrawn. The osmolarity was reduced to -700 kPa (17.1 g PEG 6000 / 100 mL MES buffer) for these internodes. As needed, each piece was then taped to a glass slide with masking tape, and placed in a bath of MES buffer. This was then placed on the stage of an Olympus BH-2 microscope (see Fig. 1B) equipped with Olympus SPlan10 10X (NA 0.30) and ULWD SDPlan20 20X (NA 0.40) objectives. The second electrode was then placed in the bath to provide a continuous electrical pathway.

All electrophysiological measurements were made with a WPI Duo-773 electrometer (World Precision Instruments, Inc., Sarasota, FL, USA) fitted with high impedance active probes (Fig.1E). Inner filamented glass microelectrodes of between 0.5 and 1 μm in diameter were made using 1 mm-diameter pipettes (WPI Kwik-fil™ K100-F3) which were pulled with a Narishige PB-7 Pipette Puller (Narishige Co. Ltd., Tokyo, Japan). These microelectrodes were back-filled with Lucifer Yellow (LYCH, 5 % w:v in 3 M LiCl) solution. The tips were allowed to fill, after which the shank was backfilled with 3 M LiCl, ensuring that no bubbles

were present in the needle, as these would impart an electrical resistance on the needle, preventing injections and electrical potential monitoring. These were then screwed into WPI (World Precision Instruments, Sarasota, Florida) LiCl filled microelectrode holders with Ag/AgCl half-cells and a side channel (Item No. MEH2SF10) (see Fig. 1F). The microelectrodes were positioned in the half-cells at the junction with the side channel, rather than being screwed all the way back. This was found to facilitate the use of the pressure injector while at the same reducing contamination of the half-cells with silicon oil and not interfering with the membrane potential measurement.

This assembly was then attached to a WPI high impedance probe, and in turn to a WPI DC3001 R motorised micromanipulater that was attached to a WPI PM10 Piezo controller. The silicon oil filled pressure injector fitting was then attached to the side channel, ensuring that no bubbles were present, as this would result in spurious pressure readings due to gas compression. Injections were performed under UV light. Injections were made into storage parenchyma, the bundle sheath, and parenchyma adjacent to the bundle sheath. When a cell was successfully impaled, The turgor pressure of the cell (in excess of 1600 kPa) forced the LYCH up the microelectrode. The pressure in the system was then increased until the LYCH was present in the tip of the needle, and it was allowed to recover for five min in the dark, by inserting a shutter in the beam path to prevent UV exposure and damage. During this period, the cells' potential and viability were monitored using the Duo773 electrometer. If the membrane potential stabilised (at least -40 mV as prescribed by Farrar *et al.* 1992, and Van

Bel *et al.* 1996), the impaled cells was reverse-iontophorised, using pulsed current (-2 to 130 nA, for 5-60 seconds) in order to inject the dye. Injections were photographed using an Olympus AD PM-10 camera system with Fujichrome Provia 400 slide film. The Olympus filter sets used were:

Table 2: Wavelength specifications in nm of the LYCH and Blue Olympus filter sets used for pressure assisted microiontophoresis.

	Exciter	Beam-splitter	Emitter
LYCH	425-440	460	540
Blue	425-440	460	540-550

All equipment, except the pressure injector, was supplied by Wirsam Scientific (Port Elizabeth, South Africa). The pressure injector was constructed in house (see Figs. 1C-D). The pressure injector, with the exception of the use of a standard microelectrode holder, is based on and functionally similar to the device described by Kempers *et al.* (1999).

Results

3.1 Anatomical studies

3.1.1 Internode 5

Figures. 2 and 3 are plates showing aspects of the anatomical detail of deep-seated tissue from internode 5 of sugar cane. Figure 2A shows a vascular bundle in the pith in TS. It has typical monocotyledonous features as discussed in the introduction. The transport phloem comprises sieve elements (SE), companion cells (CC) and phloem parenchyma (PPar). The phloem parenchyma is located directly below the sclerenchymatous sheath (SS) (which may be multilayered in places, and is associated with the phloem fibre cap), that subtends the parenchymatous bundle sheath (BS). The bundle sheath consists of large, thin-walled cells. The phloem is capped by a phloem fibre cap, which is centrifugal of the crushed protophloem (PP). This interrupts the parenchymatous bundle sheath at the centrifugal end. The bundle sheath is well defined around the centrifugal half of the vascular bundle, but tends to be unclear around the centripetal half. The xylem comprises two large metaxylem vessels, as well as a solitary protoxylem element, and an associated, well-defined, protoxylem lacunae, together with tracheary elements and parenchymatous cells around and between the metaxylem vessels, and surrounding the centrifugal end of the protoxylem element. Figure 2B shows two deep-seated vascular bundles in TS, as well as the surrounding storage parenchyma. There is some variation in storage parenchyma cell size, with larger cells being interspersed with occasional smaller cells. Even at this low magnification (300X), the wrinkled appearance of the cell end-walls can be

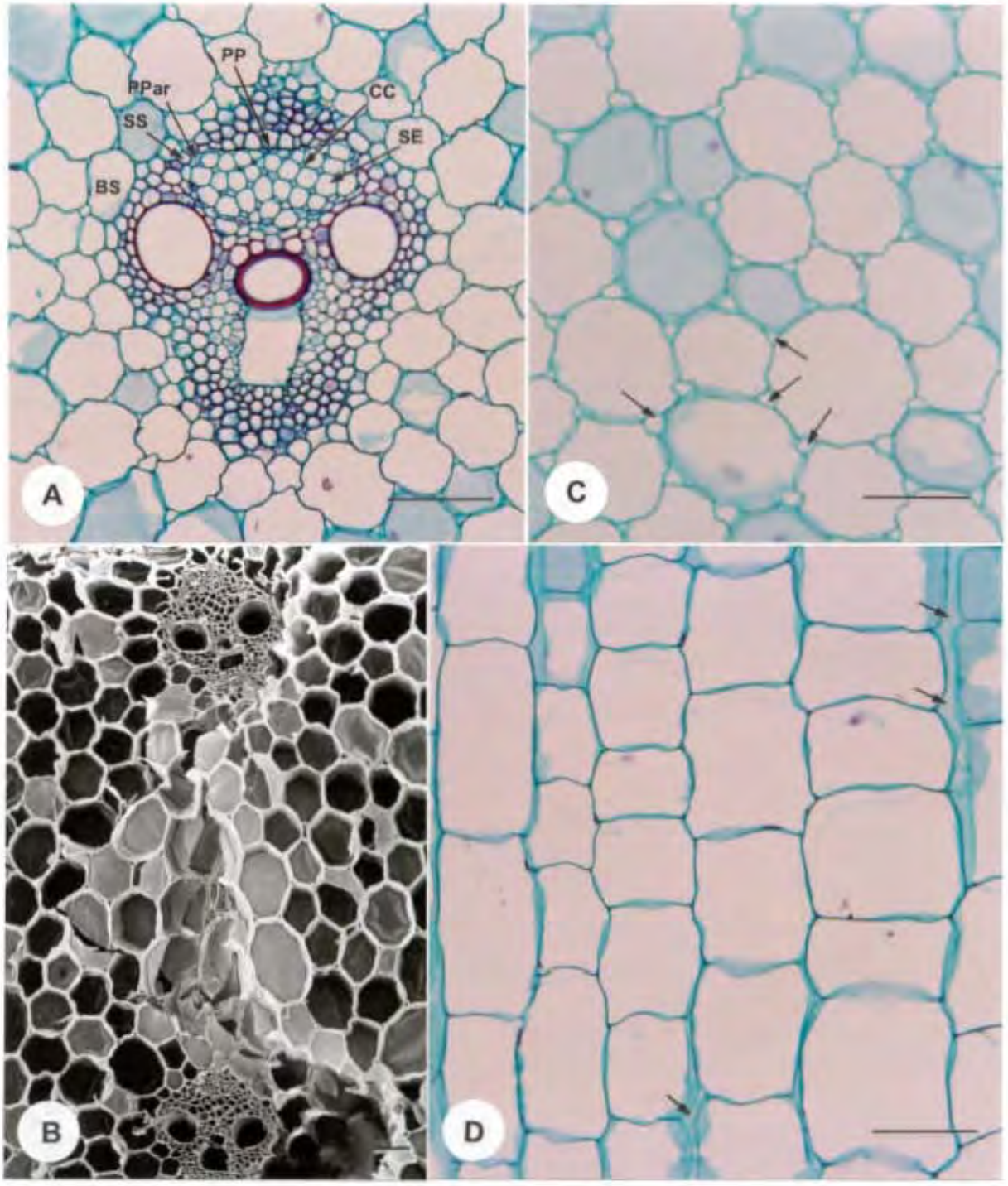
PP
PPar
CC
SS
SE
BS
A
C
B
D

Fig. 2: Shows the anatomy of internode 5. (**A**) TS of a large vascular bundle showing phloem with sieve elements (SE), small companion cells (CC), crushed protophloem (PP), and phloem parenchyma (PPar) within the sclerenchymatous sheath (SS) and parenchymatous bundle sheath (BS). (**B)** SEM in TS of the pith tissue showing two vascular bundles, and storage parenchyma showing some variation in cell size. (**C**) Shows detail in TS of the storage parenchyma. Note the intercellular spaces (arrows) and variation in cell size. (**D**) Detail of the storage parenchyma in longitudinal section showing intercellular spaces (arrows). Note the variation in cell size and shape. (A-D) Bar = 100 µm

observed. This wrinkled surface texture is caused by the physical wrinkling of the cell wall itself, which is an artefact created during critical point drying. Figures 2C and D shows storage parenchyma in transverse and longitudinal section. Large intercellular spaces (arrows) are present, suggesting the existence of a large volumed apoplasm. There is a variation in cell size visible in these and other sections. The larger storage parenchyma cells are interspersed with smaller cells, which might not be storage parenchyma cells. In Fig. 2D, which shows the storage parenchyma in longitudinal section, these smaller cells within the surrounding storage parenchyma cells are more elongated and narrower than the storage parenchyma cells. They are arranged in vertical columns of cells of approximately the same diameter suggesting that these cells extend through the length of the pith tissue and that they may have a specific function within the pith tissue. Large intercellular spaces (arrows) are visible between columns of cells.

Figure 3A shows storage parenchyma in longitudinal section. The previously noted variation in cell size and shape is again observed here. The narrow, elongate cells to the left of the micrograph are bundle sheath cells. The cell walls have a wrinkled appearance that may be an artefact of critical point drying. Broad cells alternate with narrow cells, and plasmodesmal fields occur in both. Figure 3B is a higher magnification view of a similar region. Many plasmodesmal fields (arrows) are visible. Note the longitudinal, parallel wrinkles associated with the cell walls. The larger, more obvious ones show where cell walls of adjacent cells touch the visible cell, while the other wrinkles could be

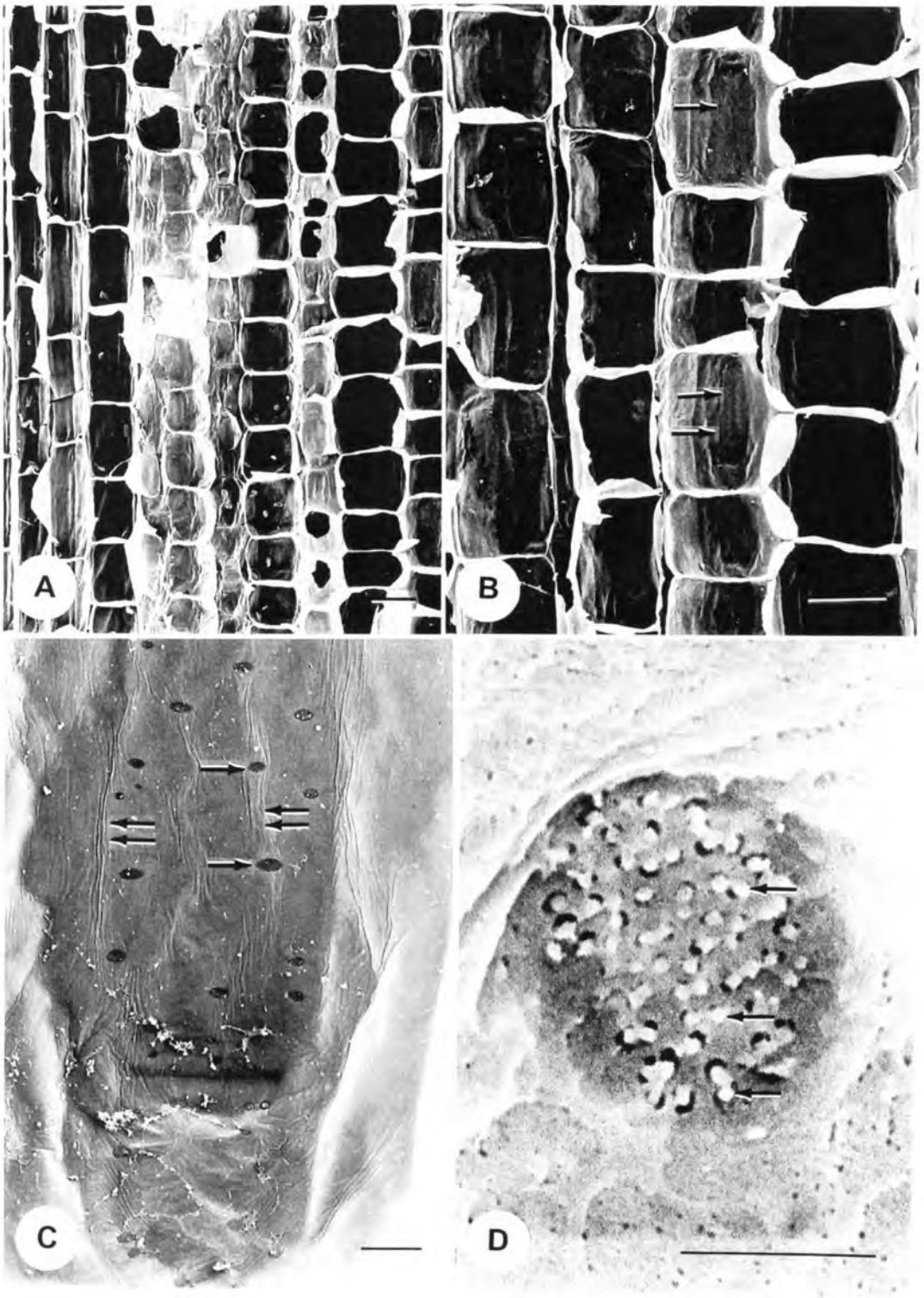
A
B
C
D

Fig. 3: Detail of internode 5 as seen with the SEM. (**A**) Longitudinal section of the storage parenchyma showing variation in cell size and shape. Note that similar-sized cells are found in vertical columns. (**B**) Shows the storage parenchyma in LS. Plasmodesmal fields (arrows) appear to be aligned with small wrinkles in the cell-wall surface. (**C**) Shows a detail in LS of part of a storage parenchyma cell showing plasmodesmal fields (arrows) and longitudinal wrinkles (paired arrows). (**D**) Shows a single end-wall plasmodesmal field at high magnification. The field contains approximately 60 plasmodesmata (arrows). (A-B) Bar = 100 μm, (C) Bar = 10 μm, (D) Bar = 1 μm

plasmamembrane folds indicative of the underlying cell wall structure. Interestingly, plasmodesmal fields appear to be aligned along these wrinkles. This association can also be seen in Fig 5D. This appears to indicate that the wrinkles in question are associated with the plasmodesmata. Figure 3C shows a single parenchymatous cell in which many plasmodesmal fields (arrows) can be seen. Note that the outlines of the plasmodesmal fields in the radial-wall are approximately ovate. The longitudinal, parallel wrinkles (paired arrows) co-associate with plasmodesmal fields. Figure 3D shows a single sunken plasmodesmal pit field in the end wall of a storage parenchyma cell. The field contains ca 60 plasmodesmata, of which three are indicated by arrows. The endoplasmic reticulum appears to be associated with the plasmodesmata within the pit and associated with the surrounding cell wall. Plasmodesmal fields in longitudinal walls of storage parenchyma on the other hand, have pits that are almost flush with the cell wall surface (see Fig. 11B).

3.1.2 Internode 7

Figure 4 shows the images of anatomical detail of deep-seated tissue from internode 7 of sugar cane. Figure 4A shows a vascular bundle in the pith in TS. Sieve elements (SE) and companion cells (CC) are visible, and the phloem parenchyma (PPar) occurs directly below the inner sclerenchymatous sheath (SS) below the parenchymatous bundle sheath (BS). Typically, two metaxylem vessels, a protoxylem element, and a protoxylem lacuna are present in the xylem, together with associated parenchyma cells and tracheids. Figure 4B illustrates the storage parenchyma in TS. Numerous intercellular spaces

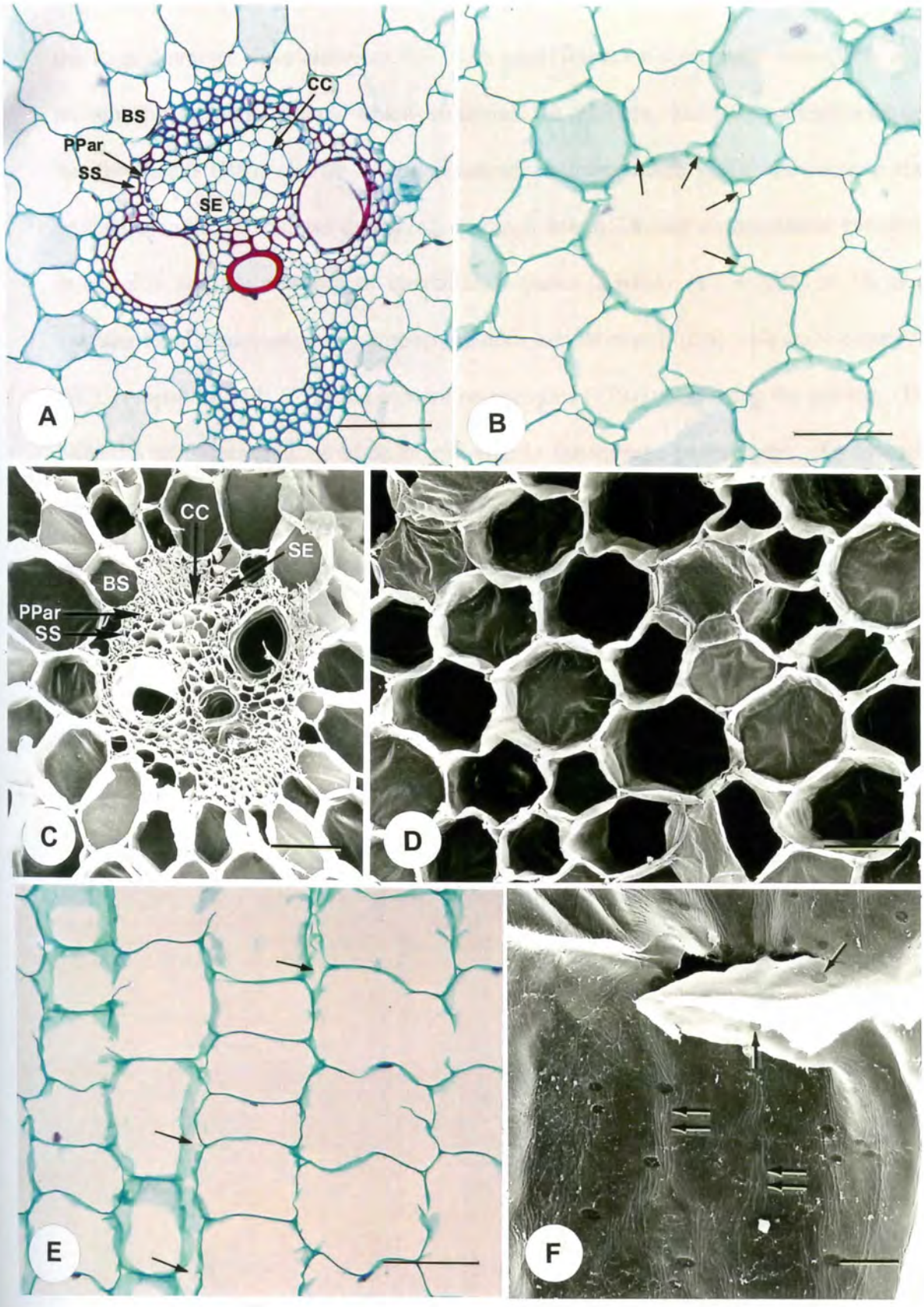
CC
BS
PPar
SS
SE
A
B
CC
SE
BS
PPar
SS
C
D
E
F

Fig. 4: Illustrates the anatomy of internode 7. (**A**) A TS of a vascular bundle showing the large diameter sieve elements (SE) with small diameter companion cells (CC), and phloem parenchyma (PPar) which comprise the phloem, and the parenchymatous bundle sheath (BS), exarch to the sclerenchymatous sheath (SS), surrounding the vascular bundle. (**B**) Shows the storage parenchyma in TS, and demonstrates variation in cell size and the presence of intercellular spaces (arrows). (**C**) A SEM in TS of a vascular bundle surrounded by parenchymatous bundle sheath (BS) with sieve elements (SE), companion cells (CC) and phloem parenchyma (PPar) comprising the phloem. (**D**) SEM TS demonstrating variation in cell size in the storage parenchyma. (**E**) Storage parenchyma in LS showing variation in cells size and shape, and demonstrating the presence of intercellular spaces (arrows). (**F**) Shows the junction between two storage parenchyma cells in detail, illustrating what could be plasmamembrane folds (paired arrows) associated with cell walls, and end-wall plasmodesmal fields (arrows) in both cells. (A-E) Bar = 100 μm, (F) Bar = 10 μm

(arrows) are present at the corners of intersections between cells, suggesting the presence of a large- apoplasmic volume. There is considerable variation in cell size, with larger cells associated with interspersed smaller cells. When observed at the SEM level (Fig. 4C), the sieve elements (SE) and companion cells (CC) can be identified, as can the associated phloem parenchyma (PPar) located directly beneath the sclerenchymatous sheath (SS) that surrounds the vascular bundle below the parenchymatous bundle sheath (BS). The xylem tissues are essentially similar to those earlier described for Fig. 4A. Figure 4D shows storage parenchyma in TS. There is some variation in cell size, with the larger cells being associated with smaller ones, as noted earlier. The wrinkled appearance of the visible end walls is most likely a preparation artefact. Figure 4E illustrates the variability of cell size and shape of the storage parenchyma in LS, with similarly shaped and sized cells being arranged in columns. Apoplasmic spaces (arrows) are present in this section. Figure 4F shows the junction between two cells from a longitudinal section of the storage parenchyma. Many plasmodesmal fields are visible, with the plasmodesmal fields in the end walls (arrows) being circular in shape, rather than ovate. As stated, plasmodesmal pit fields in the end walls are deeper than the relatively shallow depressions seen in Fig. 4F. The cell wall surface is wrinkled (paired arrows), possibly due to plasmamembrane folding which reflects the underlying cell wall structure.

3.1.3 Internode 8

Figure 5 shows anatomical detail from deep-seated storage and vascular tissues in internode 8. Figure 5A shows a vascular bundle in TS. The phloem is composed of large diameter sieve elements (SE) and relatively small diameter companion cells (CC), together with associated phloem parenchyma cells (PPar). A sieve plate (SP) is visible in this image. Large intercellular spaces are visible in the surrounding parenchyma, suggesting the presence of a substantial apoplasmic volume. The xylem is comprised of two metaxylem vessels, two protoxylem elements, and a protoxylem lacuna. Figure 5B shows the transport phloem of another vascular bundle near to that shown in Fig. 5A in more detail. A sieve plate (SP) is present, and sieve elements (SE), companion cells (CC), and phloem parenchyma (PPar) are visible in the section. Xylem parenchyma (XP) occurs on the low side of the micrograph. Figure 5C shows part of the end wall of a storage parenchyma cell in TS at high magnification. Numerous plasmodesmal fields (arrows) are visible, and appear smaller than those in Fig. 5D. Endoplasmic reticulum (ER) is visible, and forms a web like pattern across the cell wall plasmamembrane complex. Figure 5D shows part of a radial cell wall of a parenchyma cell directly adjacent to the bundle sheath taken at the same magnification as Fig. 5C. Many plasmodesmal pit fields (arrows) are visible. These plasmodesmal pit fields are again ovate as described previously. Longitudinal cell wall wrinkles (paired arrows) possibly reflect the underlying cell wall structure. The larger plasmodesmal fields seem to be arrayed in longitudinal rows. The boundary (B) between the two cells subtending the visible cells is visible in this image. Figure 5E shows a single plasmodesmal pit

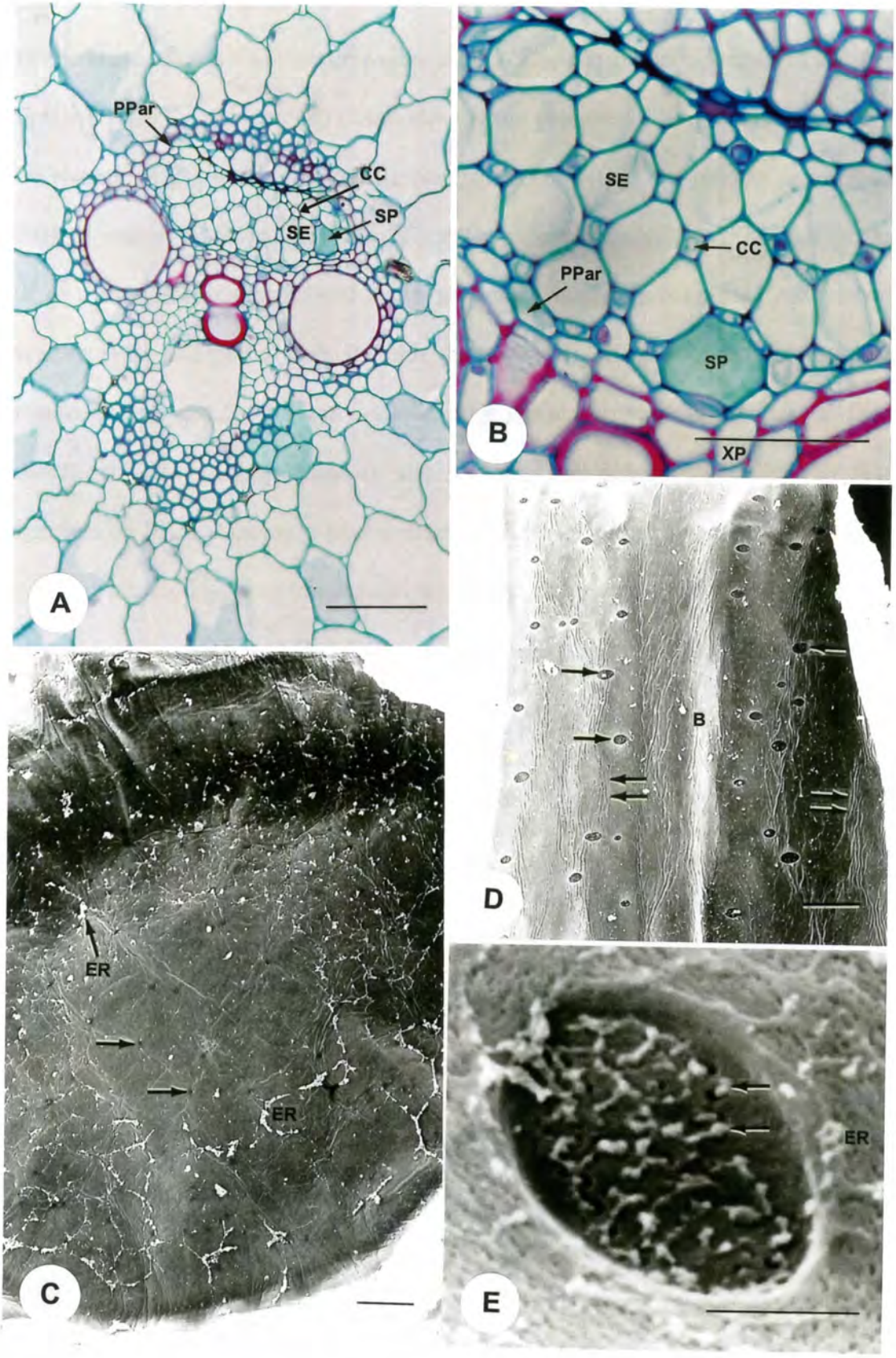
PPar
CC
SP
SE
A
SE
CC
PPar
SP
B
XP
B
D
ER
ER
C
ER
E

Fig. 5: Illustrates the anatomy of internode 8. (**A**). Shows a large vascular bundle in TS with the sieve elements (SE), companion cells (CC), and phloem parenchyma (PPar) which comprise the phloem. (**B**) Detail view of the phloem showing the large diameter sieve elements (SE), a sieve plate (SP), companion cells (CC) and phloem parenchyma (PPar), as well as xylem parenchyma (XP) in the xylem tissue. (**C**) A SEM in of the end wall of a storage parenchyma cell in TS showing reticulately-connected endoplasmic reticulum (ER) and plasmodesmal fields (arrows). (**D**) A SEM of part of a storage parenchyma cell in LS with cell wall wrinkles (paired arrows), plasmodesmal fields (arrows), and the visible boundary (B) between two subtending cells. (**E**) High magnification SEM showing a plasmodesmal field in a parenchyma cell end-wall. A number of plasmodesmata (arrows) and associated endoplasmic reticulum (ER) can be seen in this micrograph. (A) Bar = 100 μm, (B) Bar = 50 μm, (C-D) Bar = 10 μm, (E) Bar = 1 μm

field, in which approximately 90 plasmodesmata are visible, of which two are indicated by arrows. Note the associated endoplasmic reticulum (ER).

3.1.4 Internode 10

Figures 6 and 7 show aspects of the anatomical detail of deep-seated storage and vascular tissues in internode of the stalk. Figure 6A shows a large vascular bundle in TS. The phloem contains sieve elements (SE) and companion cells (CC), while the phloem parenchyma (PPar) is visible directly below the sclerenchymatous sheath. A parenchymatous bundle sheath (BS) occurs exarch to the sclerenchymatous sheath (SS). As in other internodes, large intercellular spaces (arrows) are visible in the surrounding parenchyma. Two protoxylem elements and a protoxylem lacuna are present in the xylem, in addition to two metaxylem vessels. Figure 6B shows bundle sheath (BS) and storage parenchyma (P) cells in LS. The bundle sheath cells are more elongated than the storage parenchyma cells. Plasmodesmal pit fields (PD) are visible throughout the section. Some endoplasmic reticulum (ER) is visible in the storage parenchyma cells. Figure 6C shows the storage parenchyma in LS. The variation in cell size is less marked than observed in the younger internodes. Nonetheless, a column of evidently smaller parenchymatous cells (S's) is present adjacent to the broader storage parenchyma cells. Intercellular spaces (arrows) are visible between this column of narrower cells and the storage parenchyma cells. Figure 6D shows the storage parenchyma in LS. The central cell is short and broad in shape, similar to those seen in Fig. 6C. Endoplasmic reticulum (ER) is visible on the cell wall surface. What appear to

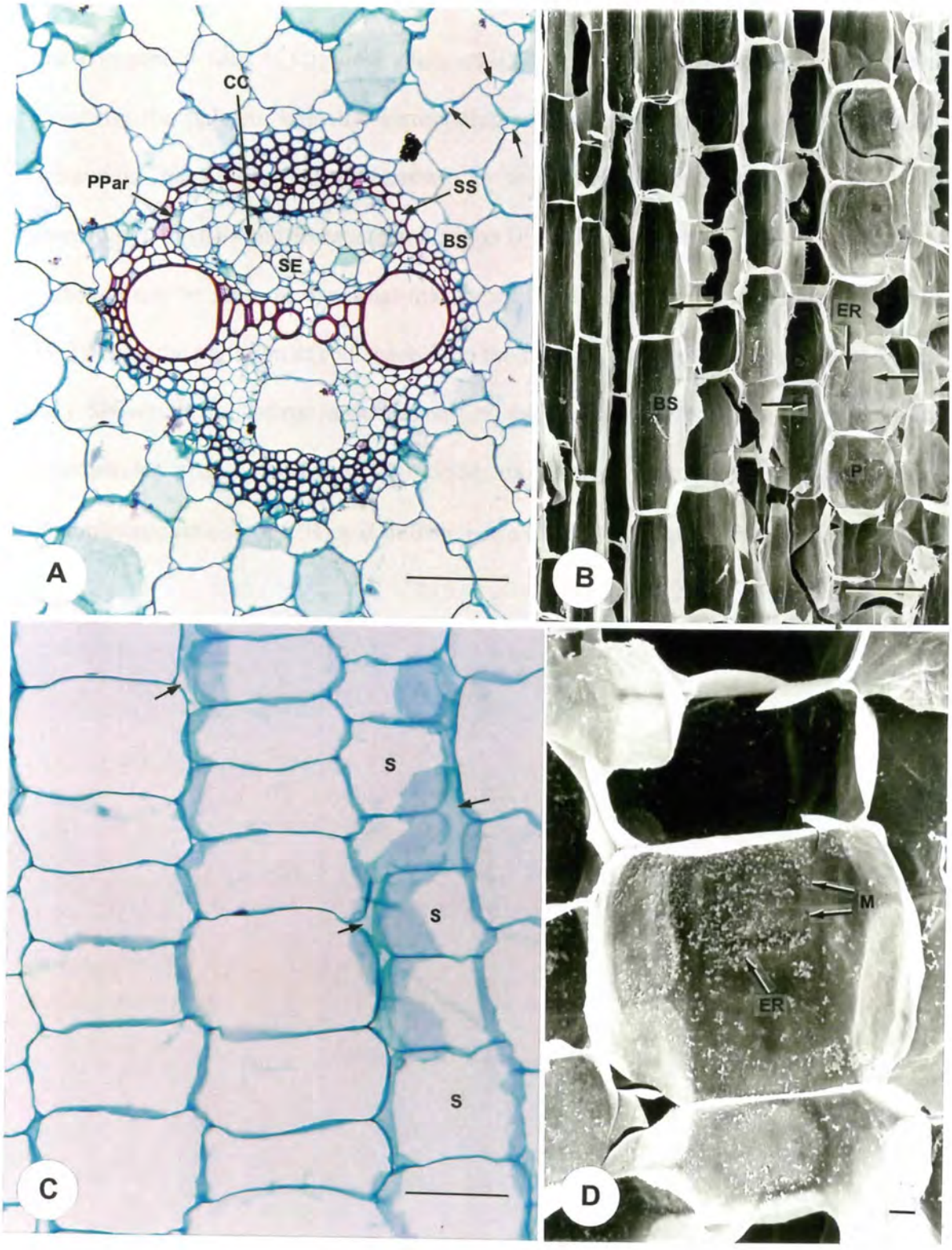
CC
PPar
SS
BS
SE
A
ER
BS
Pl
B
S
S
S
C
M
ER
D

Fig. 6: Shows the anatomy of internode 10. (**A**) A large vascular bundle in TS showing the companion cells (CC), sieve elements (SE) and phloem parenchyma (PPar) that comprise the phloem, with the surrounding parenchymatous bundle sheath (BS) and numerous intercellular spaces (arrows) in the storage parenchyma. (**B**) Shows the bundle sheath (BS) and storage parenchyma (P) in LS. Numerous plasmodesmal fields (arrows) can be seen, as can what may be cell wall-associated endoplasmic reticulum (ER). Note the variation in cell shape from the bundle sheath to the storage parenchyma. (**C**) Shows the columnar arrangement of the storage parenchyma cells (S's) with intercellular spaces (arrows). (**D**) SEM of storage parenchyma in LS showing endoplasmic reticulum (ER) and mitochondria (M). (A-C) Bar = 100 μm, (D) Bar = 10 μm

be mitochondria (M) are present, and attached to the plasmalemma. The mitochondria are larger and more regularly shaped than the endoplasmic reticulum, and can be more clearly discerned in Fig. 7A.

Figure 7A shows the same mitochondria (M) visible in Fig. 6D at high magnification. Figure 7B shows a plasmodesmal field in storage parenchyma. Individual plasmodesmata (arrows) are visible, as is the associated fenestrated endoplasmic reticulum (ER). The plasmodesmal field has an oval outline which is essentially the same as plasmodesmal fields observed in the longitudinal walls of other parenchyma cells. The cell wall surface displays the surface wrinkling possibly produced by plasmamembrane folding. Figure 7C shows a plasmodesmal field in the end wall of a parenchyma cell at high magnification. Note the membranous material associated with the plasmodesmata. The relatively deep plasmodesmal pit appears circular in shape. Figure 7D shows a smaller plasmodesmal field in the parenchyma. Plasmodesmata (arrows) are visible, as is endoplasmic reticulum (ER). This field occurs in a shallow pit.

3.1.5 Internode 13

Figure 8 shows anatomical detail in deep-seated tissues of the sugarcane stalk. Figure 8A shows a vascular bundle in TS. The transport phloem is composed of sieve elements (SE) and companion cells (CC), while phloem parenchyma (PPar) is visible directly below the sclerenchymatous sheath (SS) subtending the parenchymatous bundle sheath (BS). Note also the crushed protophloem (PP) remnants. Intercellular spaces are visible in the surrounding parenchyma,

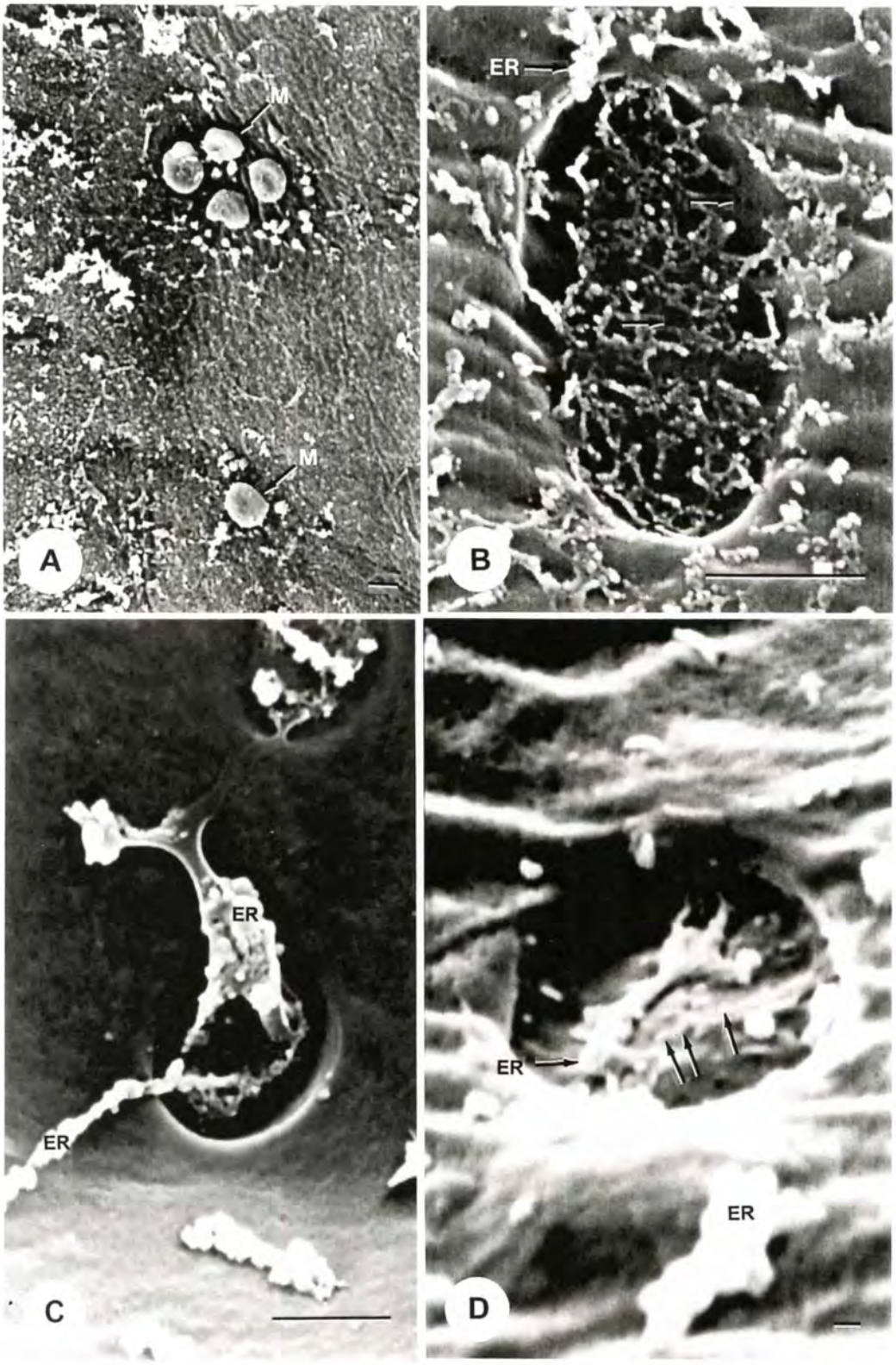
M
M
A
ER
B
ER
ER
C
ER
ER
D

Fig. 7: High resolution SEM images of cell wall details of internode 10. (**A**) A high magnification of Fig. 6D showing the mitochondria (M). (**B**) Shows the ovate outline of a radial wall-plasmodesmal field showing plasmodesmata (arrows) (**C**) Shows a detail of a plasmodesmal pit field in cell end-wall illustration the associated endoplasmic reticulum (ER). (**D**) Shows a plasmodesmal pit field in a cell end-wall. Some plasmodesmata are visible (arrows) as is the associated endoplasmic reticulum (ER), both inside and outside the pit. (A-C) Bar = 1 μm, (D) Bar = 100 nm

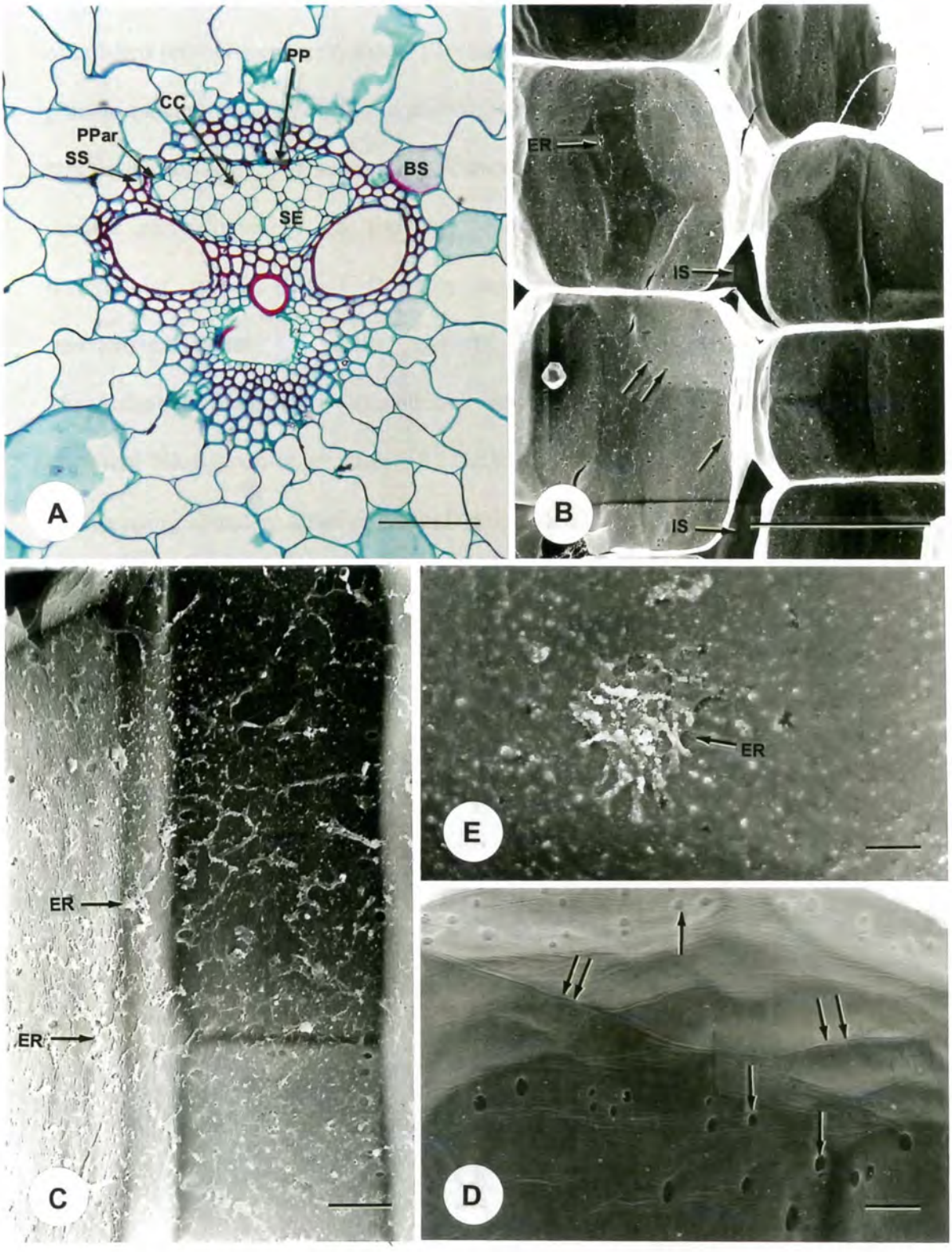
PP
CC
PPar
SS
BS
SE
A
ER
IS
B
IS
ER
ER
C
ER
E
D

Fig. 8: Anatomy of internode 13: (**A**) A vascular bundle in TS illustrating the presence of crushed protophloem remnants (PP), sieve elements (SE), companion cells (CC), and phloem parenchyma (PPar) in the phloem, as well as the surrounding parenchymatous bundle sheath (BS) and subtending sclerenchymatous sheath (SS). (**B**) SEM of the storage parenchyma in LS showing reticulate endoplasmic reticulum (ER) and intercellular spaces (IS). **C-D** show details of longitudinally sectioned storage parenchyma radial cell walls, showing attached endoplasmic reticulum (ER), plasmodesmal fields (arrows) and cell wall wrinkles (paired arrows) believed to represent plasmamembrane folds. (**E**) Detail of the end-wall of a storage parenchyma cell showing abundant attached endoplasmic reticulum (ER). (A-B) Bar = 100 μm, (C-E) Bar = 10 μm

suggesting a large apoplasmic volume. The xylem is composed of two metaxylem vessels, a protoxylem element, and an associated protoxylem lacuna is also identifiable. Figure 8B shows storage parenchyma cells in LS. Plasmodesmal fields (arrows) are abundant, as is endoplasmic reticulum (ER). Evidence of relatively large intercellular apoplasmic spaces (IS) is discernible. Figure 8C illustrates the reticulately-connected endoplasmic reticulum (ER) forming a web-like network in a storage parenchyma cell. Figure 8D shows a detail of part of a storage parenchyma cell in LS. Plasmodesmal fields (arrows) of varying sizes are visible, as is the wrinkled membrane surface texture (paired arrows) previously suggested to be plasmamembrane folding reflecting the underlying cell wall structure. Figure 8E shows part of the end-wall of a storage parenchyma cell. The light region (arrow) is a large mass of intact endoplasmic reticulum in the centre of the cell wall.

3.1.6 Internode 15

Figure 9 shows anatomical detail from stem tissues of internode 14. Figure 9A shows a vascular bundle in TS. Sieve elements (SE) and companion cells (CC) can be seen, as can phloem parenchyma (PPar), visible below the sclerenchymatous sheath (SS) surrounding the vascular bundle. The sclerenchymatous sheath is surrounded by a parenchymatous bundle sheath (BS). The protoxylem element that would form the lacuna is still intact. Many of the vascular bundles in this section do not appear to have undergone complete expansion. In contrast, the SEM image (Fig. 9B) shows a protoxylem lacuna. Figure 9B shows a vascular bundle in TS. The phloem is composed of large

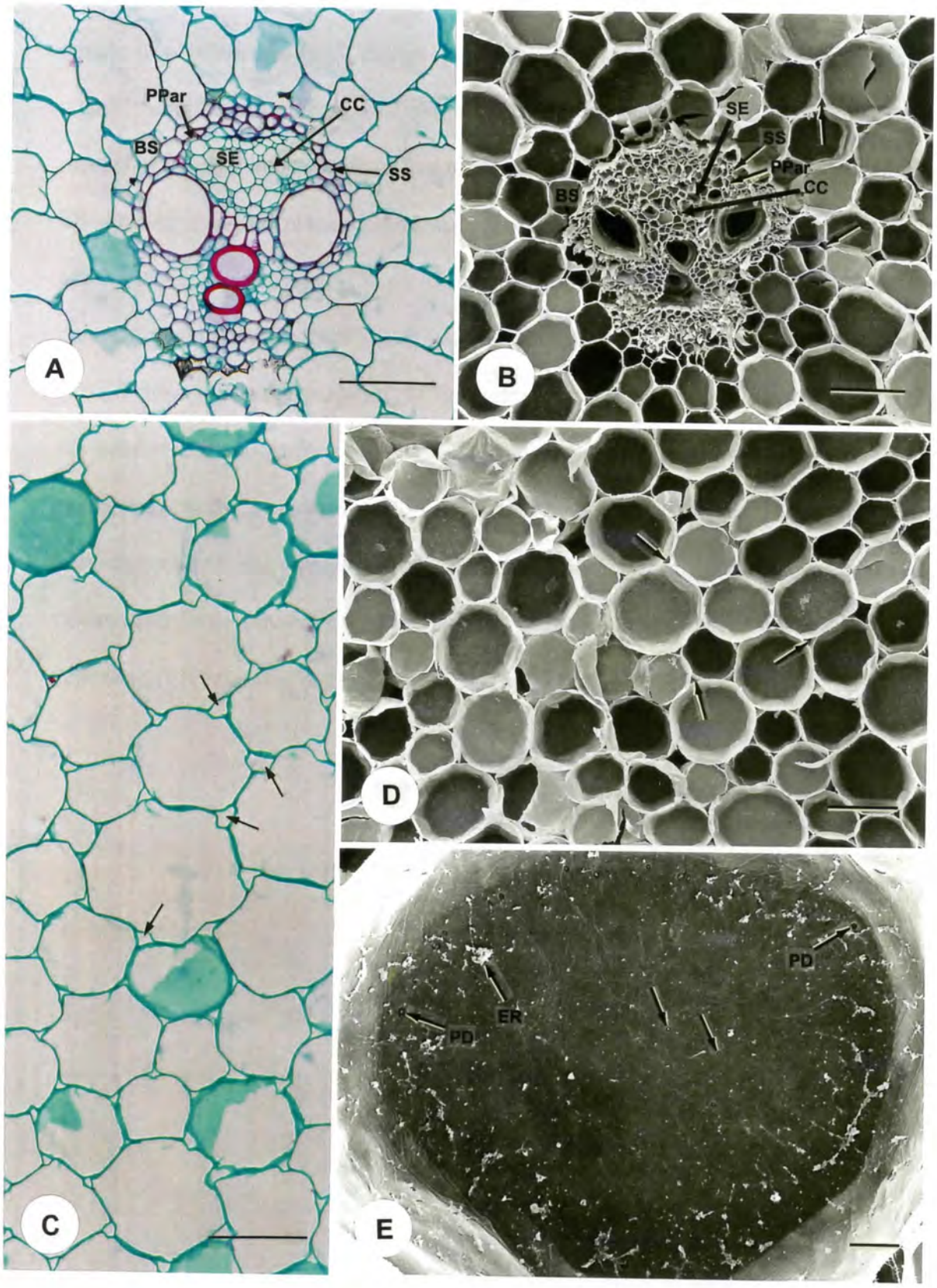
PPar
CC
BS
SE
SS
A
SE
SS
PPar
BS
CC
B
C
D
PD
ER
PD
E

Fig. 9: The anatomy of internode 15. (**A**) Shows a smaller vascular bundle in TS in which sieve elements (SE), companion cells (CC) and phloem parenchyma (PPar) which comprise the phloem, and the surrounding sclerenchymatous sheath (SS) and parenchymatous bundle sheath (BS) can be identified. (**B**) SEM of a vascular bundle in TS showing transport phloem composed of sieve elements (SE), companion cells (CC), and phloem parenchyma (PPar). Note the intercellular spaces (arrows) and the parenchymatous bundle sheath (BS) with the subtending sclerenchymatous sheath (SS). (**C**) TS through storage parenchyma illustrating the variation in cell size, and showing the intercellular spaces (arrows). (**D**) SEM showing the intercellular spaces (arrows) in the storage parenchyma tissue with varying cell sizes. (**E**) SEM image showing storage parenchyma cell end-wall in TS showing small plasmodesmal fields (arrows) in the centre, and large plasmodesmal fields (PD) near the radial cell walls. Endoplasmic reticulum (ER) can also be seen. (A-D) Bar = 100 µm, (E) Bar = 10 µm

diameter sieve elements (SE) and relatively small diameter companion cells (CC). Phloem parenchyma (PPar) is discernible directly below the sclerenchymatous sheath (SS), outside which is a parenchymatous bundle sheath (BS). A protoxylem lacuna (L) is present in the xylem, which is composed of two metaxylem vessels, a protoxylem element, tracheary elements and vascular parenchyma. Intercellular spaces (arrows) are visible in the parenchyma. Figures 9C and D show storage parenchyma in TS at the light and SEM levels respectively. Large intercellular spaces (arrows) are present, and there is a large variation in cell size. Figure 9E shows the end wall of a storage parenchyma cell in TS. Some endoplasmic reticulum (ER) is visible around the periphery of the cell wall. This is different in appearance to what was observed in Fig. 8D. Only a few small, circular, plasmodesmal fields (arrows) are visible in the centre of the cell wall. By contrast, many plasmodesmal fields (PD) can be observed in the periphery of the cell near the radial cell wall. This is also where most of the previously observed endoplasmic reticulum is concentrated. These plasmodesmal fields are also circular in shape, occurring in deep pits.

3.1.7 Motivation for the examination of, and summary of, anatomical differences between internodes

It was considered necessary to examine a range of internodes from 5 to 15 for anatomical differences that could impact on the phloem unloading and sucrose sequestration pathway. Therefore internodes 5-8, 10, 13 and 15 were selected for examination. Internode 6 was subsequently omitted from the thesis as it was

felt that it was unnecessary. On the whole, there are few differences visible at the anatomical level between the internodes examined. Older internodes were difficult to section due to the hardness of the tissue. This is evidenced by an increase in lignification of the sclerenchymatous sheath and sclerenchymatous caps relative to internode age. This was not quantified however.

3.2 Plasmodesmal associations at the TEM level

As mentioned, plasmodesmata are arranged in plasmodesmal fields. The structure of these fields varies from location to location. The plasmodesmal fields in the radial and tangential walls of the storage parenchyma cells occur in very shallow depressions or pits in the cell walls. These plasmodesmal fields are generally ovate in shape when observed at the SEM level, and there is a distinct variation in the size of plasmodesmal fields even in the same cell. The largest of these may contain 90 or more plasmodesmata. Plasmodesmal fields of greatly differing size may be found directly adjacent to each other. By contrast, the plasmodesmal fields in the end-walls of the storage parenchyma tend to be circular in shape, and are located in much deeper pits in the cell wall. There is once again a variation in plasmodesmal field size, but based on the observations, there appears to be a difference in the distribution of the different sizes. The smaller plasmodesmal fields are located in the central region of the cell wall. The larger fields are to be found at the periphery of the cell end-wall, and are frequently to be found in the radius between the radial or tangential walls, and the end-wall. Plasmodesmal fields in the parenchymatous bundle sheath vary according to their locations. Those in end-walls are circular and in

deep pits, while those connecting the bundle sheath cells to surrounding bundle sheath or storage parenchyma cells are ovate and shallow. Figures 10, 11 and 12 show details of plasmodesmal fields in deep-seated storage parenchyma and bundle sheath cells.

Figure 10A shows a shallow pitted plasmodesmal field in a semi-oblique section in the storage parenchyma of internode 5. Electron lucent collars (convergent arrows) are present on some of the plasmodesmata, suggesting that they may be occluded. Desmotubules (arrows) are visible in some of the plasmodesma. Figure10B shows a plasmodesmal field in longitudinal-section in the storage parenchyma of internode 5. Desmotubules (arrows) are clearly visible in some of the plasmodesmata. Some evidence of plasmolysis is visible which has resulted in the formation of ectodesmata, ie the partial extrusion of the plasmodesmal content. Figure 10C shows most of a plasmodesmal field in the end wall of a storage parenchyma cell in internode 6. The plasmodesmata are located in a pit, approximately 450 nm (measured as described in the Material and Methods) deep. Desmotubules (arrows) are clearly visible, as are collar-like structures (convergent arrows) which suggest that the plasmodesmata in question may be occluded. Figure 10D shows a plasmodesmal field in the end wall of a storage parenchyma cell of internode 6. Desmotubules (arrows) are present, as are collar-like structures (convergent arrows), and some plasmolysis has occurred. Two mitochondria (M) are *barely* visible adjacent to the plasmodesmal field. Mitochondria were frequently found near plasmodesmal fields, as was the case at the SEM level (see Fig. 7A).

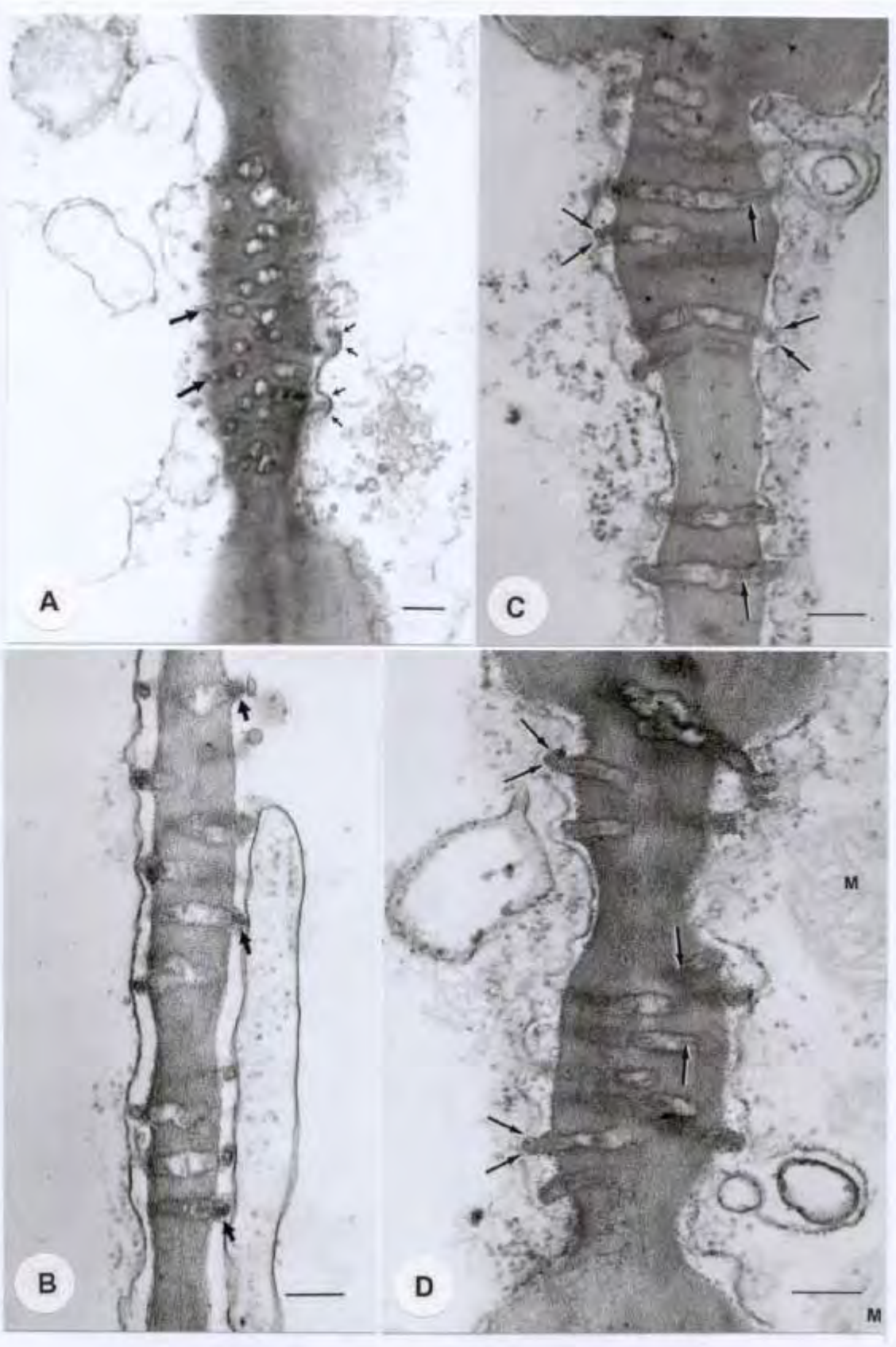
A
C
B
D
M
M

Fig. 10: Shows plasmodesmal associations at the TEM level. (**A**) Storage parenchyma plasmodesmal field in oblique section, collars associated with the neck region (convergent arrows) of the plasmodesmata, and visible desmotubules (arrows) in some plasmodesmata. (**B**) LS through a storage parenchyma plasmodesmatal field. In this instance, plasmolysis during fixation has caused the formation of ectodesmata. Desmotubules (arrows) are visible in some plasmodesmata. Collar structures (convergent arrows) are also visible. (**C**) Storage parenchyma cell end-wall plasmodesmal pit field showing desmotubules (arrows) in some plasmodesmata, as well as collar structures (convergent arrows) at the neck region. (**D**) Cell end-wall plasmodesmatal pit field from a storage parenchyma cell showing neck region collar structures (paired arrows), and desmotubules (arrows). Two mitochondria (M) are barely visible. (A-D) Bar = 200 nm

Figure 11A shows a shallow plasmodesmal field in the storage parenchyma of internode 7. The neck regions of the plasmodesmata (arrows) are notably electron dense. There is some plasmolysis in the cell to the left in the micrograph resulting in the formation of partial ectodesmata, which are still attached to the endoplasmic reticulum. Figure 11B shows plasmodesmata in a slightly oblique glancing transverse-section of a small field in either the transverse or radial wall of a storage parenchyma cell of internode 8. Desmotubules (arrows) are visible in many of the plasmodesmata, as is the bipartite structure of the plasmamembrane (paired arrows). Plasmodesmata which have darker, more electron dense centres, may have been sectioned closer to the neck region at the cell wall surface. Figure 11C shows a plasmodesmal field between the end walls of concomitant storage parenchyma cells from internode 10. The deep pit is approximately 500 nm deep, and is characteristic of plasmodesmal fields in these walls. Desmotubules (arrows) are visible in some plasmodesmata. Partial plasmolysis has resulted in ectodesmal formation. The region directly above the plasmodesmata (convergent arrows) is electron lucent, but the neck regions of the plasmodesmata are electron opaque, suggesting possible occlusion or closure of the neck region. The surrounding dark regions of the plasmamembrane are not associated with plasmodesmata, but rather are a characteristic of the interstitial plasmamembrane. Note the presence of a middle lamella.

Figure 12A shows plasmodesmata in LS in the storage parenchyma of internode 15. The desmotubule (arrows) is visible in most of these

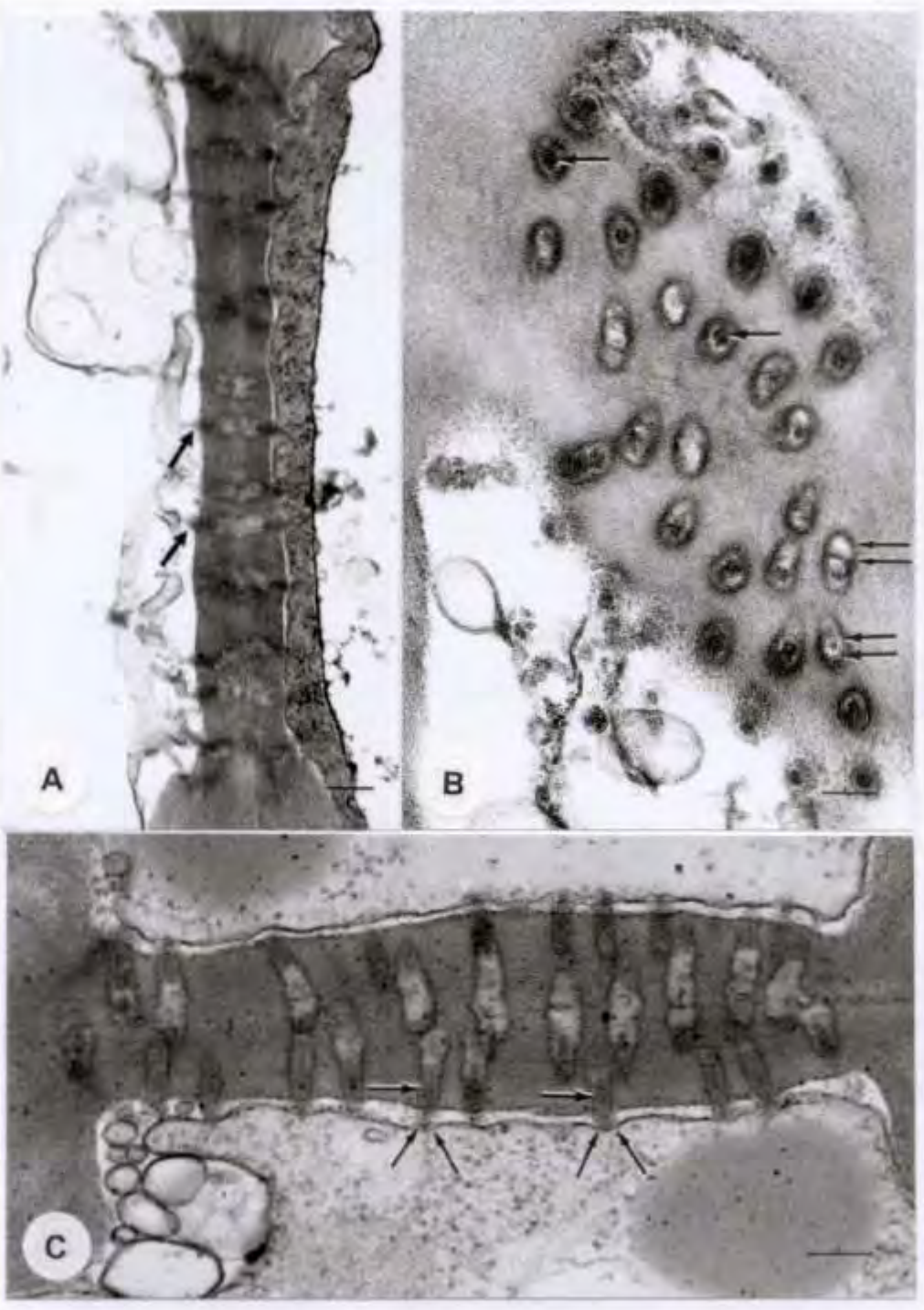
A
B
C

Fig. 11: Plasmodesmal associations at the TEM level. (**A**) Storage parenchyma plasmodesmal field showing desmotubules (arrows) (**B**) CS through a storage parenchyma plasmodesmal field showing desmotubules (arrows) and bipartite structure (paired arrows) of the plasmodesmal plasmamembrane. (**C**) Shows an end-wall plasmodesmal field between two storage parenchyma cells showing some ectodesmal formation due to plasmolysis. Electron dense regions (paired arrows) suggest possible occlusion or closure. Desmotubules (arrows) are visible in some plasmodesmata. The middle lamella can also be discerned. (A) Bar = 200 nm, (B) Bar = 100 nm, (C) Bar = 200 nm

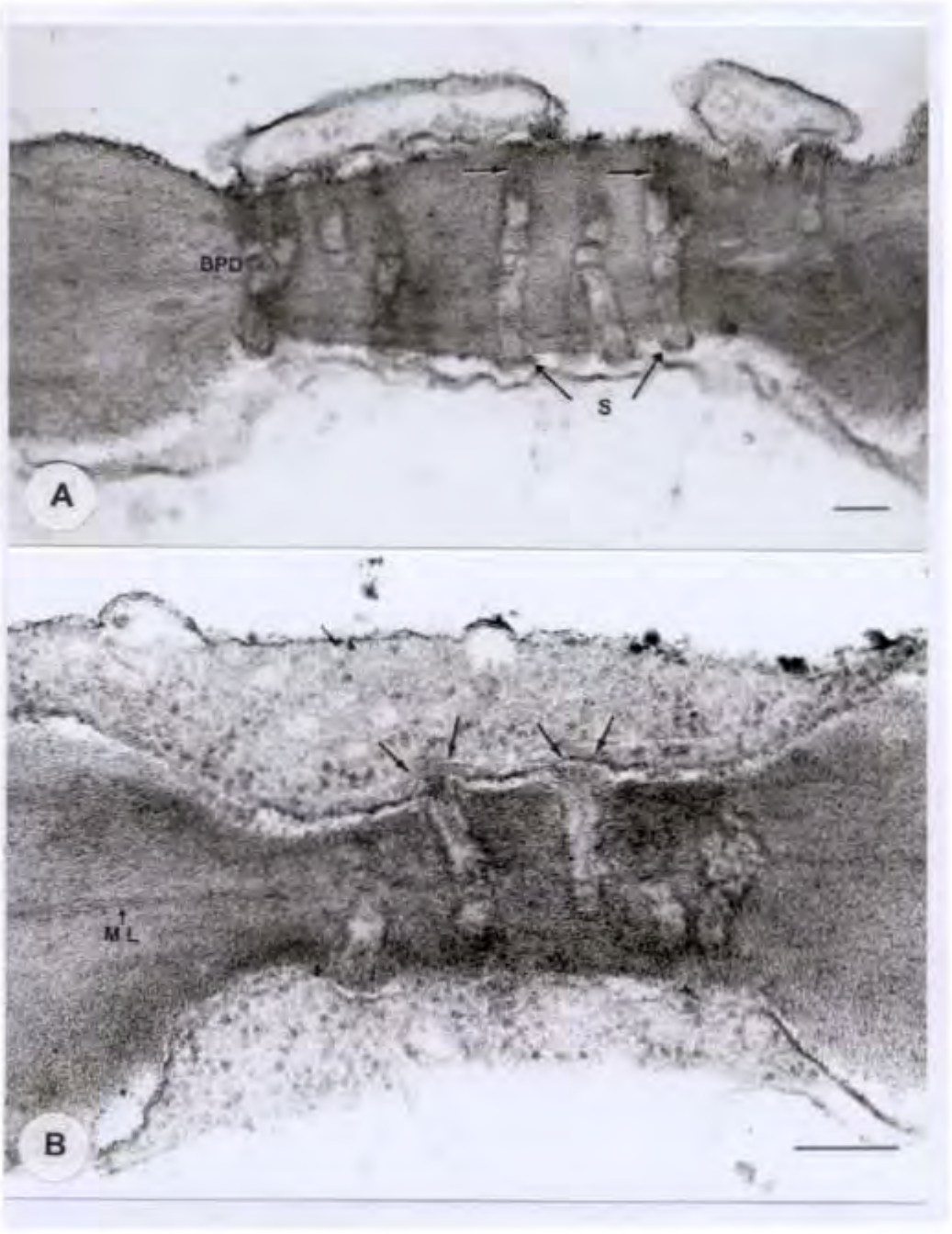
BPD
S
A
ML
B

Fig. 12: Plasmodesmal associations at the TEM level. (**A**) This plasmodesmal field communicates between a parenchymatous bundle sheath cell and a storage parenchyma cell. It displays some plasmolysis, and desmotubules (arrows) are visible in some of the plasmodesmata, and a branched plasmodesma (BPD) can also be discerned. Electron dense subunits are present in the neck region (S). (**B**) Plasmodesmatal pit field in the storage parenchyma showing collar structures (convergent arrows). Desmotubules (arrows) are visible in some plasmodesmata. A middle lamella (ML) is visible. (A) Bar = 100 nm, (B) Bar = 200 nm

plasmodesma. Note the branching plasmodesma (BPD). Some of the plasmodesmata are relatively electron lucent, and have electron dense subunits at their neck regions (S). Figure 12B shows a plasmodesmal field in the storage parenchyma. The plasmodesmal field is in a pit approximately 240 nm deep. Desmotubules (arrows) are visible in a few of the plasmodesmata. Electron dense collar structures (convergent arrows) are present in the neck region of the plasmodesmata. The necks of these plasmodesmata do not appear to be as electron dense as those of Fig. 11C. Note also the clear middle lamella (ML) at the juncture of the two cells.

3.3 Aniline blue fluorescence

3.3.1 Localisation of callose in the vascular tissue

Figure 13 illustrates callose occlusion in the phloem tissue of internodes 5 and 15 under conditions of water control, and 0.4 M and 0.9 M mannitol osmotica solutions. Figure13A shows the phloem complex of internode 5, which has been incubated in distilled water, in LS. Note the brightly fluorescing sieve plate (SP) which is occluded by callose. The parenchymatous bundle sheath (BS) can be identified. The layer with brightly fluorescing cell walls inside the parenchymatous bundle sheath is the inner sclerenchymatous sheath. Very faint fluorescence indicates the presence of callose-occluded plasmodesmal pit fields (PD). Multiple occluded pore plasmodesmal fields (arrows) can be seen in the vascular tissue, but none are visible in the bundle sheath (plasmodesmal fields may be present in these tissues, but are not fluorescing). Figure 13B shows the phloem of internode 15, also incubated in distilled water, in LS. The

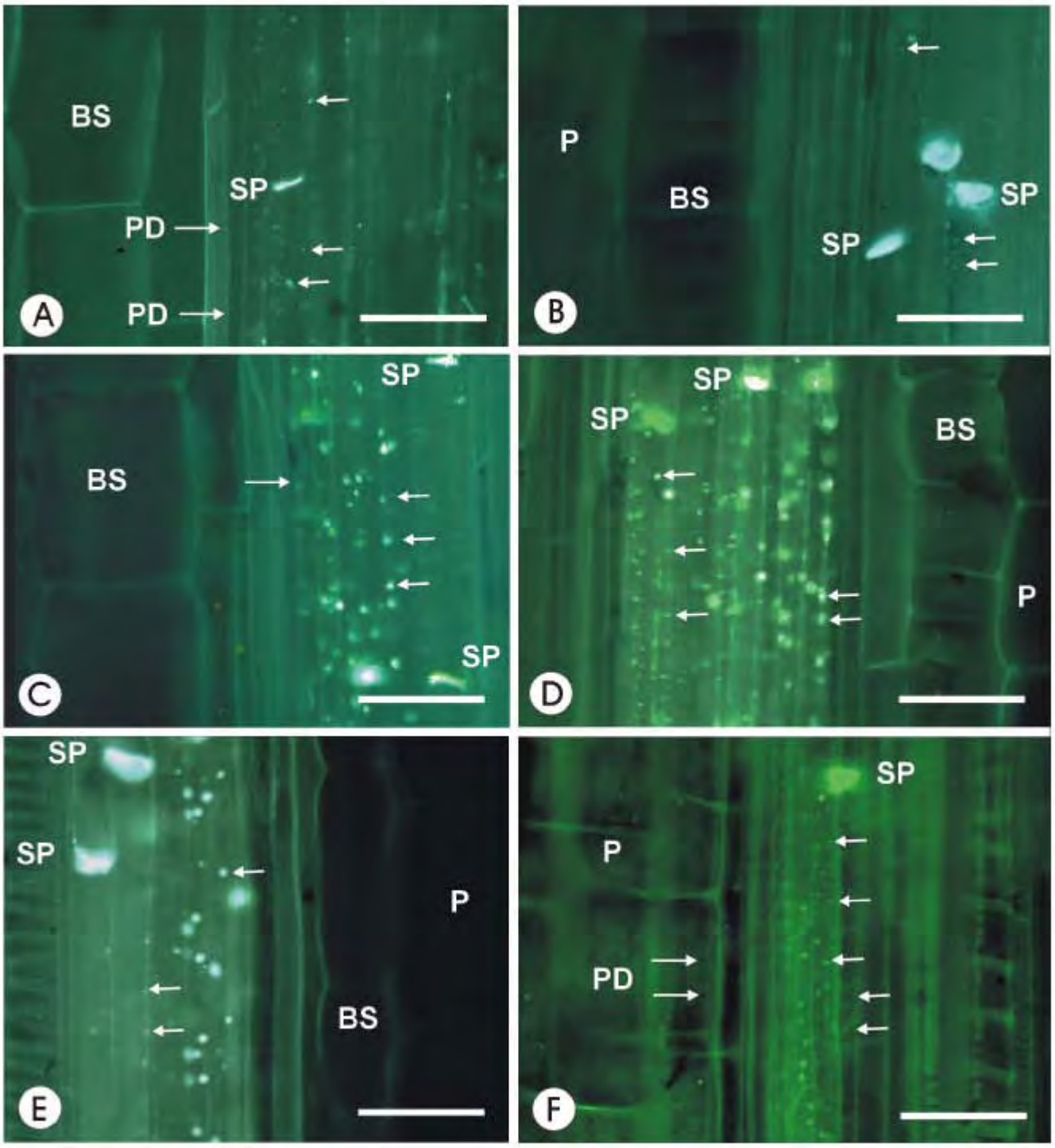
BS
SP
PD
PD
A
P
BS
SP
SP
B
BS
SP
SP
C
SP
SP
BS
P
D
SP
SP
BS
P
E
SP
P
PD
SP
F

Fig. 13: Shows the localisation of callose in the vascular tissue under various buffer regimes. A, C and E are of internode 5, while B, D, and F are of internode 15. (**A**) Shows internode 5 in H_2O. From left to right, the parenchymatous bundle sheath (BS) and phloem can be identified. Fluorescing callose-occluded pore plasmodesmal fields (arrows) and an occluded sieve plate (SP) are visible in the phloem. Faint fluorescence indicates the presence of callose-occluded plasmodesmal pit fields (PD). (**B**) Shows internode 15 in H_2O. The parenchymatous bundle sheath (BS) and phloem occur from left to right. Bright fluorescing callose-occluded sieve plates (SP) are visible in the phloem, callose-occluded pore plasmodesmal fields (arrows) can be seen. (**C**) Shows internode 5 in 0.4 M mannitol solution. From left to right, the parenchyma (P), bundle sheath (BS), and phloem are visible. Brightly fluorescing callose-occluded pore plasmodesmal fields (arrows) and sieve plates (SP) are visible in the phloem. This is in comparison to (**D**), which shows internode 15 in 0.4 M mannitol + 50 m*M* Ca^{2+}. The parenchyma (P), bundle sheath (BS), and phloem can be identified from right to left. Abundant bright fluorescence indicates the presence of many callose-occluded pore plasmodesmal fields (arrows) and sieve plates (SP). (**E**) Shows internode 5 in 0.9 M mannitol. From right to left, the parenchyma (P), bundle sheath (BS) and transport phloem can be seen. Callose-occluded sieve plates (SP) and callose-occluded pore plasmodesmal fields (arrows) are present throughout the phloem. (**F**) Shows internode 15 in 0.9 M mannitol + 50 m*M* Ca^{2+}. The parenchyma (P) is to the left of the phloem, which displays callose-occluded pore plasmodesmal fields (arrows) and an occluded sieve plate (SP). Non-fluorescing plasmodesmal fields (PD) indicating an absence of callose are visible at the bundle sheath to parenchyma interface. (A-F) Bar = 100 µm

parenchyma (P) and parenchymatous bundle sheath (BS) can be discerned. Several callose-occluded sieve plates (SP) can be seen in the sieve tubes, as can callose-occluded pore plasmodesmal fields (arrows).

Figure 13C shows the phloem tissue of internode 5 after incubation in 0.4 M mannitol. Callose occluded sieve plates (SP) are visible in the sieve elements, and callose occluded pore plasmodesmal fields (arrows) can be seen throughout the phloem tissue. The parenchymatous bundle sheath (BS) can be discerned. Figure 13D shows the vascular tissue of internode 15 incubated in 0.4 M mannitol containing 50 m*M* Ca^{2+}. The callose fluorescence is brighter due to the greater deposition of callose in the Ca^{2+} treatment. Several callose-occluded sieve plates (SP) can be seen, as can many callose-occluded pore-plasmodesmal fields (arrows). The sclerenchymatous sheath surrounding the vascular bundle inside the parenchymatous bundle sheath (BS) (To the left of the bundle sheath in the image) can be identified by the strong fluorescence of its lignified cell walls. A layer of storage parenchyma (P) can also be seen.

Figure 13E shows the vascular tissue of internode 5 following incubation in 0.9 M mannitol. Storage parenchyma (P) is present outside the parenchymatous bundle sheath (BS). The sclerenchymatous sheath can be seen to the left of the bundle sheath. Many callose-occluded pore-plasmodesmal fields (arrows) can be seen in the phloem, as may be callose occluded sieve plates (SP). Figure 13F shows the vascular tissue of internode 15 after incubation in 0.9 M mannitol + 50 m*M* Ca^{2+}. Faint fluorescence indicates the presence of callose-occluded

pore-plasmodesmal fields (arrows). Faint fluorescence associated with a callose-occluded sieve plate (SP) can also just be made out. Storage parenchyma (P) is present. This overlaps with the location of the parenchymatous bundle sheath. Plasmodesmal fields (PD) which do not show fluorescence are visible in the parenchyma, and appear to co-join the bundle sheath.

3.3.2 Callose occlusion in the storage parenchyma

Figure 14 illustrates callose occlusion in the storage parenchyma of internodes 5 and 15 in 0.4 M and 0.9 M mannitol osmotica solutions Figure 14A shows the storage parenchyma (P) of internode 5 after incubation in 0.4 M mannitol. Many callose-occluded plasmodesmal fields (arrows) are visible throughout this image. Figure 14B shows the storage parenchyma of internode 15 after incubation in 0.4 M mannitol + 50 m*M* Ca^{2+}. Callose occluded plasmodesmal fields (arrows) are visible in the column of narrow cells. No callose occluded plasmodesmal fields can be seen in the adjacent storage parenchyma cells (P) which appear to be much broader than those cells in which the plasmodesmal fields are visible. This micrograph was taken with a blue filter set as specified in the Materials and Methods.

Figure 14C shows the storage parenchyma of internode 5 following incubation in 0.9 M mannitol osmoticum. Many callose occluded plasmodesmal fields (arrows) are present in the central column of cells. This is not the case in the surrounding storage parenchyma cells (P) which appear to be broader and

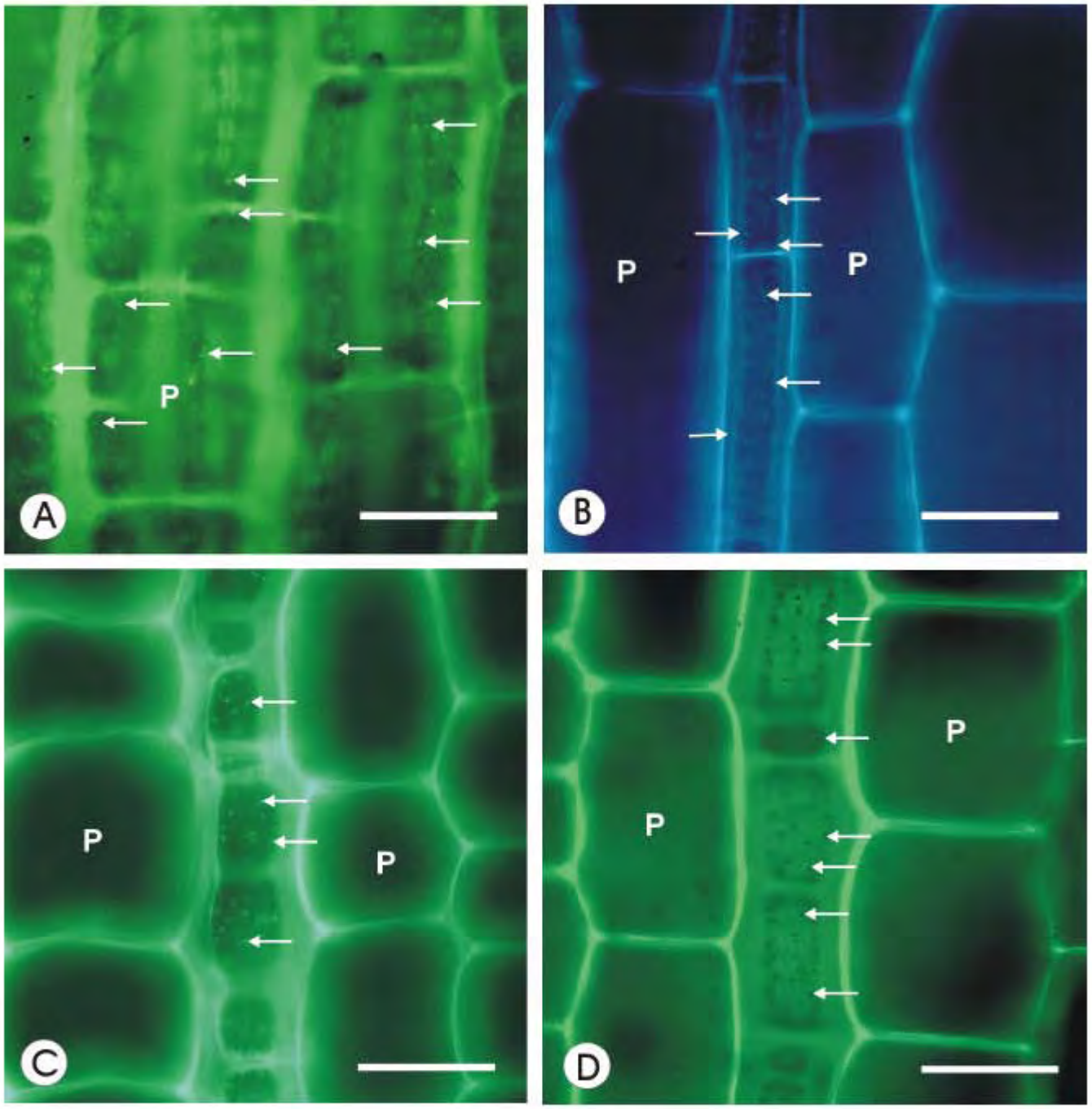
A
P
B
P
P
C
P
P
D
P
P

Fig. 14: Shows the localisation of callose in the storage parenchymatous tissue of internodes 5 (A and C) and 15 (B and D) under different buffer regimes. (**A**) Shows internode 5 in 0.4 M mannitol showing callose-occluded plasmodesmal fields (arrows) in the storage parenchyma (P), in comparison to (**B**) which shows internode 15 in 0.4 M mannitol + 50 m*M* Ca^{2+} (blue filter set). Some callose-occluded plasmodesmal fields are visible, but the fluorescence is confined to the narrow column of cells, while the surrounding parenchyma cells (P) show no sign of callose fluorescence. (**C**) Shows callose-occluded plasmodesmal fields confined to narrow column of cells within the storage parenchyma (P) of internode 5 in 0.9 M mannitol. (**D**) Shows non-fluorescing plasmodesmal fields (arrows) in the central column of cells in the storage parenchyma (P) of internode 15 in 0.9 M mannitol + 50 m*M* Ca^{2+}. (A-D) Bar = 100 µm

longer. Figure 14D shows the storage parenchyma (P) of internode 15 after incubation in a 0.9 M mannitol osmoticum solution containing 50 m*M* Ca^{2+}. Non-fluorescing plasmodesmal fields are visible (arrows) in the central column of cells.

3.4 Pressure-assisted microiontophoresis

Figure 15 shows three microinjection events in deep-seated vascular and storage parenchyma tissues in the internodal stem tissue of NCo376, showing both the presence and absence of transport. Figures 15A-B are UV fluorescence micrographs of an injection event into the parenchyma adjacent to the bundle sheath in internode 10. Figure 15B was taken five min after Fig. 15A. The brightly-lit cell is the injected cell in both images. Some longitudinal (arrows) and lateral transport has occurred. These cells have previously been shown to be connected by abundant plasmodesmal fields. The lateral transport is into the parenchymatous bundle sheath characteristic of the examined plant. In Fig. 15B, recorded five min later, further longitudinal movement of the LYCH (vertical arrows) has been recorded, causing the cell above the injected cell, which is towards the apex of the plant, to fluoresce brighter. Lateral movement of LYCH (horizontal arrow) has occurred to the cell on the lower left-hand corner. Figure 15C is a high magnification image of a single injected cell in the storage parenchyma of internode 15. No transport has occurred. This is typical of results obtained in pressure injection experiments on sugar-cane stem tissue, where individual cells can be loaded with LYCH, but no further transport occurs. Due to the small volume occupied by the cytoplasm versus the much larger

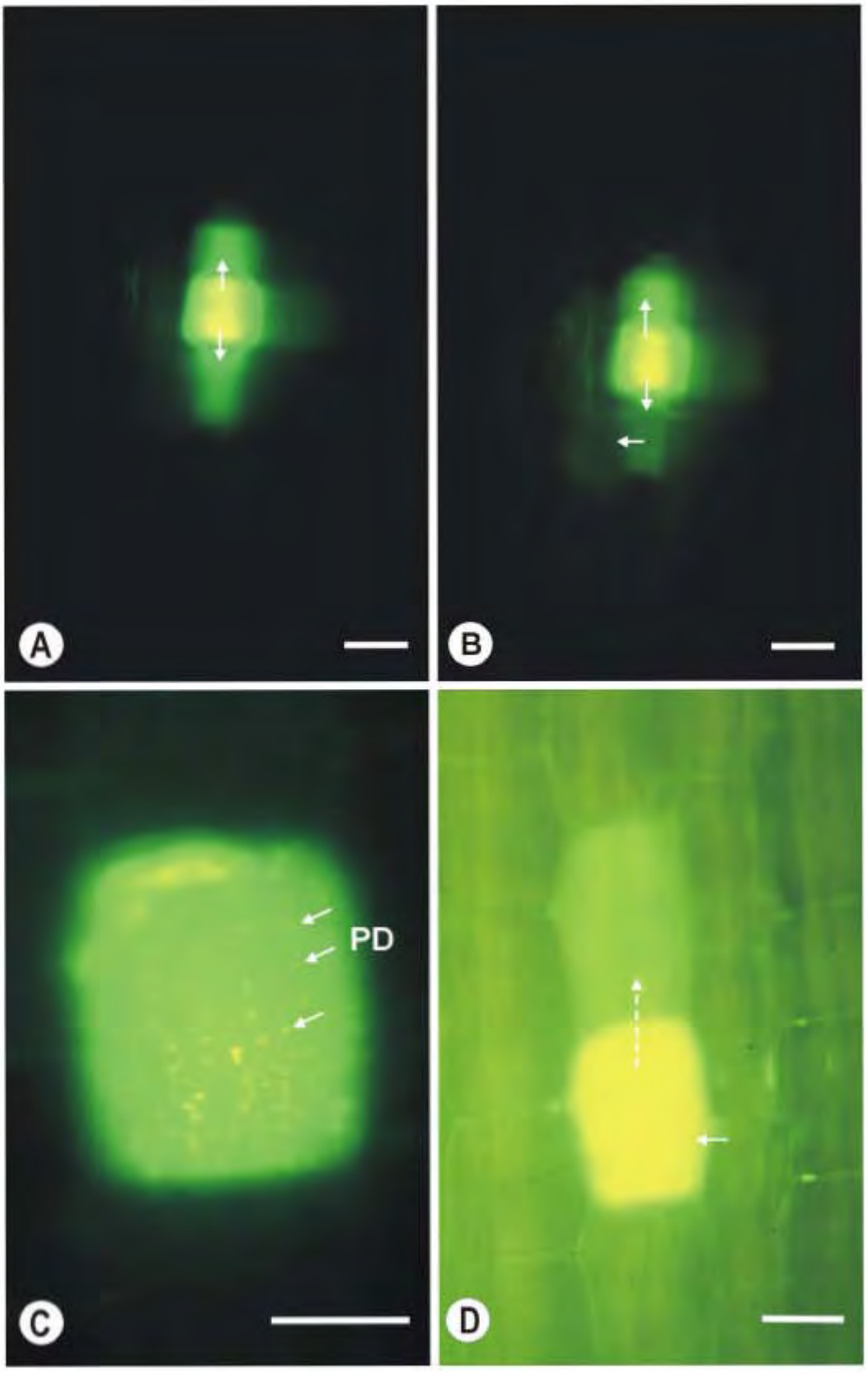
A
B
PD
C
D

Fig. 15: Shows images obtained through pressure-assisted microiontophoretic studies. **A-B** show an injection event sequence. (**A**) Shows the injection into the parenchyma adjacent to bundle sheath in internode 10. The brightest cell is the stabbed one. Some lateral transport of LYCH has occurred, but visible transport is primarily in a longitudinal direction (arrows). (**B**) Shows the same injection event after 5 min during which the tissue was not exposed to UV light. A small amount of further longitudinal transport of LYCH (vertical arrows) has occurred, but most of the transport has been laterally to the parenchyma (horizontal arrow) at the lower end of the injected cell. (**C**) Shows an injection event into a storage parenchyma cell of internode 15. No transport has occurred, but bright speckles indicate the positions of plasmodesmal fields (PD), which are identifiable by both their size and distribution. (**D**) Shows an injection event into another storage parenchyma cell from internode 15. The brightly fluorescing cell (arrow) was injected, This was followed by the immediate longitudinal transport of LYCH (dashed arrow) to the dimmer cell. (A-C) Bar=50 μm, (D) Bar=100 μm

vacuole, successful injection of the cytoplasm is difficult. This image demonstrates an injection into the narrow cytoplasm of the cell. Bright speckles indicate the presence of plasmodesmal fields (PD). These are be identified by their size, and distribution in longitudinal rows (compare with plasmodesmal fields in Figs. 3C, 4F, 5D, 6B, and 8E). The actual site of fluorescence is probably the endoplasmic reticulum associated with the plasmodesmal field, to which the LYCH may bind (Pers. com. CEJ Botha 2000). Figure 15D is an injection into the parenchyma of internode 15. The brightly fluorescing cell was injected, and immediate transport occurred to the fainter cell. Transport then ceased. This image suggests the presence of limited symplasmic transport, as the direction of transport precludes a leak when the needle is withdrawn through a previously pierced cell. Although this was probably an injection into the vacuole for reasons previously discussed, LYCH is confined to the symplasm in non-leaking injections. This movement of LYCH can only have occurred via the plasmodesmata connecting the symplasmic volumes of the two adjacent cells. This is the sole occurrence of transport in the deep-seated parenchymatous tissue from a total of 291 attempted injections.

3.4.1 Analysis of difficulties encountered with microiontophoresis

The very limited transport observed in the dye-coupling experiments has several possible causes. First, it is possible that no symplasmic connectivity exists at the injected locations. However, the SEM studies demonstrate the potential for transport at these localities. Many plasmodesmal fields are present

in regions representative of injected locations. Potential for symplasmic transport therefore exists within storage parenchyma.

Secondly, aniline blue reactions provide evidence of callose occlusion under osmotic stress in some regions, with scant evidence of callose occlusion elsewhere in the parenchyma. Less callose was observed as the buffer concentration was increased from 0.4 M mannitol to 0.9 M mannitol. As sectioning aniline blue examination is carried out under buffer, this suggests that the plasmodesmata connecting the storage parenchyma were normally closed, preventing change in turgor pressure between adjoining cells.

Thirdly, it is possible that sugarcane is not amenable to microinjection studies other than using very immature growth stages. The plant cell vacuoles may occupy 90 % of the cellular volume (Boller & Wiemkin 1986). The cytoplasm must thus be confined to the margins of the cell, and will be very narrow, typically 400 nm in the storage tissue. At the setting used to produce microelectrodes, the tip diameter is approximately 1 μm. This diameter is more than double the thickness of the cytoplasm in fully turgid NCo376 storage parenchyma cells. It could therefore be that attempts to inject would pierce the vacuole and the cytoplasm. Vacuolar injections are effectively inevitable in the more mature internodes of NCo376 from internode 5 onwards. Microinjection cannot be considered to be a useable technique in this situation.

Both the second and third explanations appear to pertain in this situation. However, explanation three must be regarded as being the overriding problem. This negates the likelihood of any injection-dye-coupling experiments working as required.

Discussion

4.1 Vein anatomy of NCo376

Light and SEM studies showed that the deep-seated vascular bundles of NCo376 possess well-defined phloem, which consists of large diameter sieve element with small, nearly square companion cells. The xylem comprised two large metaxylem vessels, tracheids, and (usually) a single protoxylem element with an associated lacuna. Phloem parenchyma was observed inside the sclerenchymatous sheath. This sclerenchymatous sheath forms an unusual boundary between the phloem parenchyma and the parenchymatous bundle sheath. If this was leaf tissue, it might be termed a mestome sheath (Hattersley and Watson 1976).

4.2 Significance of the sclerenchymatous sheath

Most members of the NADP-ME *Andropogonanae* do not have mestome sheaths, but some (*S. officionarum*, the closely related *Erianthus fastigus*, and *Chrysopogon cylindrica* and *Imperata cylindrica*) have a variable condition where some veins possess a mestome sheath and some do not (Hattersley & Watson 1976). The sclerenchymatous sheath was noted by Jacobson *et al.* (1992) as being impervious to the apoplasmic transport of water. As such it may be considered to be a stem-based equivalent to the mestome sheath found in sugarcane leaves (Eastman *et al.* 1988). The presence of a mestome sheath-like layer may preclude an apoplasmic transport pathway from the phloem to the parenchymatous bundle sheath exarch to the sclerenchymatous sheath. If a single pathway of solute transport were assumed, then the presence of the

sclerenchymatous sheath would likely necessitate a symplasmic pathway at this juncture. However the presence of the sclerenchymatous sheath in no way precludes the possibility of an operational post-bundle sheath apoplasmic pathway.

Callose occlusion was observed via aniline blue reactions at the interface between the phloem parenchyma and sclerenchymatous sheath, suggesting that the symplasm is normally contiguous at this point (see Fig. 13A), and under the control of plasmodesma. Large plasmodesmal fields were visualised at this interface under SEM. Aniline blue is assumed to react with callose deposited after sectioning due to loss of turgor pressure in sectioned cells (Oparka and Prior 1992) and possible accompanying plasmolysis following mannitol induced osmotic stress.

Evert *et al.* (1977) noted that the bundle sheath cells in leaves of *Z. mays* L are suberised, suberisation being observed between adjacent bundle sheath cells, and between bundle sheath cells and vascular parenchyma. Plasmodesmata traverse the suberised cell walls, suggesting the presence of a symplasmic pathway at these locations. It may be assumed that the bundle sheath of this species functions in a similar fashion to the suberised sclerenchymatous bundle sheath observed in *Saccharum* stems by Walsh *et al*. (1996) by forcing a symplasmic step (loading) step between parenchymatous tissue and the vascular tissue. This layer was identified by Jacobsen *et al*. (1991) as an apoplasmic barrier to the movement of solutes in *Saccharum* stem tissue. Note

that this layer is identified in this study as a sclerenchymatous sheath subtending a parenchymatous bundle sheath. Botha *et al.* (1982) demonstrated that Prussian blue crystals were confined to the veins of *Themeda triandra* leaves previously treated with 0.05 % ferrous sulphate (w/v, in distilled water). The suberin lamella in the outer walls of the bundle sheath prevented the apoplasmic transport of the aqueous ferrous sulphate, and thus prevented the formation of Prussian blue deposits outside the veins. The sclerenchymatous sheath may also function in a similar fashion to the root endodermis, given that it is both sclerified and suberised. This would not only force a symplasmic step in the unloading pathway, but might also function as a barrier against apoplasm-borne pathogens (Schreiber *et al.* 1999).

4.3 Observations based on anatomical studies

A trend of increased lignification of the sclerenchymatous caps and sclerenchymatous sheath related to internode age was observed from internode 5 to internode 15, which confirms the observations of Jacobson *et al.* (1992) and Walsh *et al.* (1996). Figure 9A (internode 15) shows a smaller, unexpanded vascular bundle in which less lignification appears to present that the trend suggests, but in Fig. 9B, which shows a normal large bundle, this trend of increased lignification is visible.

LS and TS sections of the storage parenchyma show some variation in the size of cells, as wells as large intercellular spaces, which suggest the possibility of a large volumed-apoplasm. The variation in cell size may be of significance in

certain regions of the storage parenchyma as evidenced by the localisation of callose occluded plasmodesmal fields to narrow cells located in columns through regions of larger cells which show little or no sign of callose occlusion.

4.4 Plasmodesmal fields as related to potential symplasmic connectivity

The presence of abundant plasmodesmal fields demonstrates at least the potential for a symplasmic transport pathway within the storage parenchyma. Plasmodesmata were seen in all tissue regions examined with the SEM, including the sclerenchymatous sheath and the concomitant parenchymatous bundle sheath. High magnification micrographs of individual plasmodesmal fields in the parenchyma demonstrated the presence of 60-90 individual plasmodesmata per field. Individual plasmodesmata were visible as pronounced protuberances when viewed with the SEM (see Figs. 3D, 5E, and 7E). These protuberances could be the collar structures also observed in Figs. 10A, 10C, 10D, and12B, and as observed by Robards and Lucas (1990), Botha and Cross (2000), and others. Both Botha and van Bel (1992) and Evert *et al.* (1996) used plasmodesmal frequency to predict phloem-loading pathways. The presence of abundant plasmodesmal fields in the storage parenchyma of sugarcane suggests that a potential symplasmic pathway exists between the cells.

A curious phenomenon noted during the examination of SEM images in longitudinal view an apparent association between plasmodesmal fields and cell wall-surface wrinkles. These wrinkles could either be artefacts of preparation, or they could equally be due to the underlying topography of the cell wall's

microfibrillar structure (Pers. com CH. Bornman 2001) which may cause the plasmamembrane to become locally folded. Of interest as well was the fact that there appeared to be two different plasmodesmal field shapes in the walls of storage parenchyma cells. Ovate outline fields within shallow pits were found in the side walls, and an apparently smaller, circular outline within deeper pits was found in the end-walls.

4.5 Ultrastructural studies

Protruding collar structures in the neck region of the plasmodesmata were observed in most instances (see Figs. 10A, 10C, 10D and12B, for example). The constricted neck regions of the plasmodesmata were electron dense, while the surrounding collar-like structure is electron lucent. A thick layer of granular electron dense material was frequently seen in the plasmodesmal pit (see Figs. 10C, 10D, 11A and12B, for example). This material appears to be absent from SEM images, suggesting that it may either be a preparation artefact, or that it is removed during SEM preparation. The presence of the collars, and the associated neck constrictions suggests that the plasmodesmata were gated (shut), possibly by callose occlusion (Moore-Gordon *et al.* 1998). Fig. 12A, which shows a plasmodesmal field connecting a parenchymatous bundle sheath cell to a storage parenchyma cell, has some plasmodesmata in which the neck region is relatively electron lucent, with electron dense subunits being present on either side of the neck. Botha *et al.* (1993) reported that the plasmodesmata at the kranz mesophyll-bundle sheath interface in *Themeda triandra*, possessed electron lucent regions, specifically between the

cytoplasmic sleeve and the desmotubule. They speculate that this represents open space available for symplasmic transport. The visible desmotubules in NCo376 would suggest that these plasmodesmata displays an open and unoccluded appearance (Botha and Cross 2000). Furthermore, the presence of mitochondria near plasmodesmal fields also suggests a functional relationship.

Botha and Cross (2000) speculate that the electron dense material comprising the collar structures contains callose, in addition to other electron dense proteins. Callose is usually reported as being electron lucent (Robards and Lucas 1990). Smith and McCully (1978) suggest that the translucency of callose may be due a more open structure which permits better resin infiltration, and in turn preventing the penetration of heavy metal stains (i.e. lead citrate and osmium tetroxide used in this study).

4.6 Aniline blue fluorescence

4.6.1 The situation in vascular tissue

Stem sections from internodes 5 and 15 (Figs. 13A and B, respectively), which had been sectioned under water, and mounted in aniline blue dissolved in water, show much less visible fluorescence than sections from 0.4 M and 0.9 M mannitol osmotica. These were expected to show much more fluorescence, given the difference in osmotic and turgor pressures between the tissue and the water. Welbaum *et al.* (1992) noted that the osmolarity of storage tissue from internode 10 was 0.8 MPa in greenhouse grown sugarcane. It is possible that the plasmodesmata were already occluded, perhaps with the electron lucent-

dense matrix referred to by Botha and Cross (2000). Massive fluorescence from callose-occluded sieve plates and pore plasmodesmal fields would be expected, given phloem's sensitivity to damage (van Bel 1999). Incubation and sectioning under 0.4 M mannitol osmoticum resulted in much more fluorescence, indicating an increase in the deposition of callose. This is visible in both internodes 5 (Fig. 13C) and 15 (Fig. 13D), with an apparently greater deposition of callose in internode 15. Both the mannitol osmoticum and the aniline blue dye solution (made up in 0.4 mannitol osmoticum) used for internode 15 results presented contained 50 m*M* Ca^{2+}. The increased fluorescence in Fig. 13D compared to Fig.13C suggests a possible allosteric interaction with 1,3-β-glucan synthase stimulated an increase in the deposition of callose (Kauss 1987). When 0.9 M mannitol osmoticum was substituted for the 0.4 M osmoticum, lower apparent fluorescence were observed for both internodes 5 and 15 (Figs. 13E and F, respectively). The difference in apparent fluorescence between Figs. 13C and E appears to be minor and may be largely due to the sectioning angle through the vein. The apparent difference between Figs. 13D and F appears to be greater, with less bright fluorescence in the phloem for tissue incubated and sectioned in 0.9 M mannitol osmoticum. Both samples were incubated in an osmoticum containing 50 m*M* Ca^{2+}. It appears that the deposition of callose has been inhibited under the 0.9 M mannitol osmoticum regime within the sugarcane stalk tissue. This may be due to a greater difference in osmotic pressures between tissue and osmotica solutions for the 0.4 M mannitol osmoticum than for the 0.9 M mannitol osmoticum. This may result in a more pronounced wounding response in tissue from internode 5

which was incubated in the 0.9 M osmoticum than for internode 15 (Hughes and Gunning 1980, Lucas *et al.* 1993).

The presence of non-callose-occluded plasmodesmal fields at the parenchyma-parenchymatous bundle sheath interface in Fig.13F suggests that the plasmodesmata at this crucial junction (see Jacobsen *et al.* 1992 and Walsh *et al.* 1996) are normally closed. This contradicts published literature, but is supported by other observations. It is possible that closure is effected by a non-callosic mechanism, such as the deposition of proteins, such as the extraplasmodesmal electron dense material reported by Botha and Cross (2000, Figs. 3A-D). Dissimilar granular deposits, filling plasmodesmal pits rather than simply surrounding the plasmodesmal necks, but nonetheless electron dense, and possibly proteinaceous, were observed in several plasmodesmal fields (see Figs. 11C and 12B, for example). Interestingly, Wright and Oparka (1997) suggest that the plasmodesmata connecting the sieve elements and companion cells with the parenchyma and pericycle cells in *Arabidopsis* roots are usually non-functional, but may open under different physiological conditions. Occluded plasmodesmal fields were seen at the sclerenchymatous sheath-phloem parenchyma interface (PD) in Fig. 13A, which suggests that the plasmodesmata at this location are normally gated open. The activation of the wounding response due to the loss of turgor pressure has resulted in the closure of these plasmodesmata by the deposition of callose (Hughes and Gunning 1980, Lucas *et al.* 1993).

4.6.2 The situation in storage parenchyma

When parenchymatous tissue was examined under 0.4 M mannitol osmoticum, callose-occluded plasmodesmal fields were observed throughout Fig. 14A (internode 5). Cell wall-surface fluorescence appears to indicate that callose has been deposited on the cell walls in addition to the plasmodesmal fields. When viewed with the SEM microscope (see Figs. 3B and 3C), longitudinal cell wall-surface wrinkles were observed, and the plasmodesmal fields appeared to be aligned along them. Within the cells (see Fig. 14A), callose-occluded plasmodesmal fields are visible. The fields are arranged in rows, which agrees with the images obtained at the SEM level (see Fig. 3C, for example). This suggests that callose has not been deposited in the wrinkled region, but rather in the smooth regions between. Figs. 14B, C, and D, appear to represent similar regions in the parenchyma, possibly indicating that the parenchyma in sugarcane is not physiologically and anatomically uniform. In Fig.14B, which shows internode 15, the callose-occluded plasmodesmal fields are confined to a column of narrow cells. Fluorescence other than the normal cell wall autofluorescence appears to be completely absent from the surrounding large storage parenchyma cells, indicating the absence of callose deposition. However, SEM studies showed that plasmodesmal fields were abundant throughout the parenchyma. The apparently contradictory result suggests that the plasmodesmal fields in this region are either not susceptible to callose occlusion, or are somehow (permanently) gated closed with some other substance. The second option is more likely, as the first would make the tissue more vulnerable to damage (from continuous loss of turgor pressure and the

resultant plasmolysis in the event of the rind being broken for example). A similar situation can be observed in Fig.14C, where once again the fluorescence indicating the presence of callose-occluded plasmodesmal fields is only present in a localised column of cells, with the surrounding tissues showing no evidence of callose deposition. In Fig.14D (internode 15, 0.9 M mannitol buffer, 50 m*M* Ca^{2+}), the presence of multiple non-fluorescing plasmodesmal fields confined to a localised column of cells suggests that the symplasm is no longer open. This is consistent with Patrick (1997), who concluded that plasmodesmal conductivity in plants unloading along axial paths (such as sugarcane) would decrease in parallel with changes in the source-sink balance. This would eventually result in an exclusively apoplasmic unloading pathway. The author noted that unloading by bulk flow was more important in species such as sugarcane, which accumulate osmotically active solutes (such as sucrose) behind apoplasmic barriers. It is possible that the narrow cells represent isolated symplasmic domains within the storage parenchyma in which the plasmodesmata are functional for longer than in the surrounding storage parenchyma.

4.7 The calcium effect

Smith and McCully (1978) questioned whether aniline blue in fact has any specificity for 1,3-(-glucan, normally assumed to be callose. The authors noted that (at the time of publication) the only demonstrated link between callose and 1,3-β-glucan was the demonstration by Aspinall and Kessler (1957,cited by Smith and McCully, 1978) that *Vitis vinifera* sieve plates contain a 1,3-β-glucan.

Smith and McCully point out that the fluorochrome may have bound to uronic acid residues. However, Eleftheriou (1990, cited by van Bel 1999) observed that callose deposition did not always occur in monocotyledons, even though it was a ubiquitous phenomenon in dicotyledonous species. This was also demonstrated by Botha and Cross (2000). Van Bel (1999) speculated that this questions the universal validity of callose deposition as a mechanism of sieve element control by occlusion. The addition of Ca^{2+} results in an increase in the deposition of callose due to the allosteric interaction of 1,3-β-glucan synthase (Kauss 1987). This would appear to indicate that callose (as the term is used in this research) is in fact 1,3-β-glucan. Eschrich *et al.* (1965, cited by van Bel 1999) observed that callose deposition following injection of calcium chloride did not prevent the longitudinal movement of ^{14}C-labelled-photoassimilates. This would suggest that deposited callose does not completely occlude sieve plates. This finding might be favourably compared to suggestions by Smith and McCully (1978) that callose may have a more open structure than cellulose.

4.7.1 Plasmodesmal control by calcium-induced callose occlusion

Holdaway-Clarke *et al.* (2000) found that microiontophoretic injection of Ca^{2+} into the cytoplasm of *Zea mays* L. cv. Black Mexican Sweet resulted in the rapid closure of plasmodesmata (measured by the increase in electrical resistance), followed by their gradual opening over a timeframe of 10 seconds. This indicates that Ca^{2+} is responsible for plasmodesmal control, as suggested by Olesen and Robards (1990). They suggested that local increases in cytosolic Ca^{2+} might cause the rapid deposition of callose around the plasmodesmal neck

sphincter by glucan synthase using cytosolic UDP-glucose as a substrate. This would result in the sphincter molecules compressing the cytoplasmic sleeve subunit particles, causing them to become more closely packed, and resulting in the closure of the plasmodesmal neck. Blackman *et al.* (1999) demonstrated that a centrin-like protein is localised and concentrated around the neck regions of plasmodesmata. The authors suggest that centrin is a component of a plasmodesmal neck region control mechanism composed of calcium sensitive contractile nanofilaments, which facilitates the regulation of intercellular transport by conformational changes induced by calcium flux. Ca^{2+} is a secondary messenger (Brownlee *et al.* 1999), in that while it causes callose deposition via the allosteric interaction with 1,3-β-glucan synthase (Kause 1987), it is not the primary messenger that carries the signal for the increase in callose.

4.8 Evidence from pressure-assisted microiontophoresis

Very little evidence of symplasmic transport was obtained using this technique. Figs. 15A and 15B provide some evidence that symplasmic transport takes place in internode 10. In this injection into the parenchymatous bundle sheath, both longitudinal to other bundle sheath cells, and lateral transport to the parenchyma and sclerenchymatous sheath occurred. This contradicts aniline blue fluorescence evidence presented here, which does not show any callose deposition in this region. This location was however shown to have abundant plasmodesmal fields, which in turn would appear to suggest that plasmodesmata at this location are normally gated closed by a non-callosic

mechanism. Clearly there is some symplasmic transport capacity at this location. The only evidence obtained for symplasmic connectivity in the deep-seated storage parenchyma was for internode 15 (see Fig.15D). Symplasmic transport, or at the least symplasmic leakage, occurred from the brightly fluorescing injected cell to the dimly fluorescing cell in a longitudinal direction. Whether this represents real transport capacity, or is an aberration, is unknown for reasons discussed below.

4.9 Constriction and closure of plasmodesmata

Radford *et al.* (1998), working on roots, observed that the neck regions of plasmodesmata from roots of *Allium cepa* L. treated with 2-deoxy-D-glucose (to inhibit callose formation) were funnel-shaped. The authors suggest that these plasmodesmata were gated open by the absence of occluding callose. These authors suggest that the neck closure of plasmodesmata by deposition of callose does not form part of a control mechanism in the symplasmic pathway. Waigmann and Zambryski (2000) observed that approximately 20 % of plasmodesmata in *Abutilon* nectary trichomes displayed neck constrictions, while in the remainder, the plasmamembrane and desmotubule were straight over the entire length. Radford *et al.* (1998) found that the frequency of neck constriction was increased by dissection. This is consistent with the wounding response noted by Hughes and Gunning (1980) and Lucas *et al.* (1993). However, Ding *et al.* (1992) demonstrated that plasmodesmata of *Nicotiana tabacum* L. var. Maryland Mammoth fixed by freeze-substitution displayed neck constrictions. This suggests that the appearance of plasmodesmata may be

variable, and is dependent on the situation, location, and species. Waigmann *et al.* (1997) found that *Nicotiana clevelandi* trichome plasmodesma displayed neck constrictions, while mesophyll plasmodesmata showed and electron-lucent ring in the center. Oparka and Prior (1992) demonstrated that the induction of a pressure differential between adjacent cells of *Nicotiana clevelendi* leaf trichomes caused the closure of the connecting plasmodesmata. This was inferred by observing the symplasmic movement of injected Lucifer Yellow, in relation to induced pressure changes. Roberts *et al.* (1997), working on sink leaves of *Nicotiana benthamiana* found that carboxyfluorescein was symplasmically unloaded to the mesophyll until the sink-source transition, after which the plasmodesmata involved in the observed symplasmic transport ceased functioning.

4.10 Conclusions

The use of microiontophoresis should not be considered for use on sugarcane beyond very young internodes (younger than five), or on any species with a high cell-turgor pressure. The penetration of cells with high turgor pressures results in an immediate loss of pressure in the cell, resulting in turn in rapid deposition of callose, which prevents the symplasmic movement of injected macromolecules. In addition, care needs to be taken that the needle tip diameter does not exceed the thickness of the cytoplasm. It appears that care needs to be taken in matching up this technique with suitable species for study.

A baffling result from this study is the lack of visible callose occlusion of the plasmodesmal fields in the storage parenchyma when the tissue was sectioned under water and stained with aniline blue dissolved in distilled water. Some callose occlusion of storage parenchyma plasmodesmal fields was observed when sectioning took place in mannitol osmotica. It is possible that the plasmodesmata in the storage parenchyma of the tissue used were already occluded. Another possibility is that the tissue selected was already senescent. This was alluded to by Patrick (1997), who suggested that the plasmodesmata of mature tissues of axial phloem unloading species such as sugarcane might be non-functional, forcing an apoplasmic unloading-pathway. This may be a function of the overall age of the plant, not just the age of the internode. This intriguing merits possible investigation.

The null hypothesis employed in this study was successfully falsified. The evidence presented suggests that the symplasm is not the primary transport pathway employed in sucrose sequestration in *Saccharum* var. NCo376, and that the post-bundle sheath transport pathway is apoplasmic. This is strongly suggested by the general lack of visible callose occlusion in the storage parenchyma. Correctly, the techniques used can only determine that the pathway is not symplasmic, leaving the apoplasmic pathway as the only alternative. As claimed by previous researchers (see Jacobson *et al.* 1992, Walsh *et al.* 1996), the phloem unloading pathway from the sieve elements via the phloem parenchyma to the sclerenchymatous sheath (called the bundle sheath by these researchers) in NCo376 appears to be symplasmic.

In my opinion, the issue of apoplasmic *VS* symplasmic transport has been an outstanding issue in sugarcane research since the late 1950's. Most work has assumed a uniform transport pathway, resulting in contradictory results. The existence of a symplasmic pathway to the bundle sheath is reconfirmed in this thesis, while the presence of a non-symplasmic, hence apoplasmic sucrose sequestration pathway is consistent with current research on the physiology of sugarcane (Pers. com. Botha FC 1999). Further study on the sucrose sequestration pathway in sugarcane should be directed at active trans-cell wall transport of sucrose.

Literature cited

Aloni B, Wyse RE, Griffith S (1986) Sucrose Transport and Phloem Unloading in Stem of *Vicia faba*: Possible Involvement of a Sucrose Carrier and Osmotic Regulation. Plant Physiol. 81: 482-486

Artschwager E (1925) Anatomy of the vegetative organs of sugar cane. J. Agri. Res. 30: 196-221

Aspinall GO, Kessler G (1957) The structure of callose from the grape vine. Chem. Indus. London: 1296 (not seen)

Bieleski RL (1960) The physiology of sugar-cane III. Characteristics of sugar uptake in slices of mature and immature storage tissue. Aust. J. Biol. Sci. 13: 203-219

Bieleski RL (1962) The physiology of sugar-cane V. Kinetics of sugar accumulation. Aust. J. Biol. Sci. 15: 429-444

Blackman LM, Harper JDI, Overall RL (1999) Localisation of a centrin-like protein to higher plant plasmodesmata. Euro. J. Cell Biol. 78: 297-304

Boller T,Weimkin A (1986) Dynamics of vacuolar compartmentation. Ann Rev Plant Physiol. 37: 137-164

Botha CEJ, Evert RF, Cross RHM, Marshall DM (1982) The Suberin Lamella, a Possible Barrier to Water Movement from the Veins to the Mesophyll of *Themeda triandra* Forsk. Protoplasma 112: 1-8

Botha CEJ, Evert RF (1988) Plasmodesmatal distribution and frequency in vascular bundles and contiguous tissues of the leaf of *Themeda triandra.* Planta 173: 433-441

Botha CEJ, van Bel AJE (1992) Quantification of symplastic continuity as visualised by plasmodesmograms: diagnostic value for phloem-loading pathways. Planta 187: 359-366

Botha CEJ, Hartley BJ, Cross RHM (1993) The Ultrastructure and Computer-enhanced Digital Image Analysis of Plasmodesmata at the Kranz Mesophyll-Bundle Sheath Interface of *Themeda triandra* var. *imberis* (Retz) A. Camus in Conventionally-fixed Leaf Blades. Ann. Bot. 72: 255-261

Botha CEJ, Cross RHM (1997) Plasmodesmatal frequency in relation to short-distance transport and phloem loading in leaves of barley (*Hordeum vulgare*). Phloem is not loaded directly from the symplast. Physiol. Plant. 99: 355-362

Botha CEJ, Cross RHM (2000) Towards reconciliation of structure with function in plasmodesmata - who is the gatekeeper? Micron 31: 713-721

Bowen JE, Hunter JE (1972) Sugar Transport in Immature Internodal Tissue of Sugarcane II. mechanism of sucrose transport. Plant Physiol. 49: 789-793

Brownlee C, Goddard H, Hetherington AM, Peake L-A (1999) Specificity and integration of responses: Ca^{2+} as a signal inpolarity and osmotic regulation. J. Exp. Bot. 50: 1001-1011

Bull TA, Glasziou KT (1963) The evolutionary significance of sugar accumulation in *Saccharum*. Aust. J. Biol. Sci. 16: 737-742

Chapleo S, Hall JL (1989) Sugar unloading in roots of *Ricinus communis* L. New Phytol. 111: 391-396

Cosgrove DJ, Cleland RE (1983) Solutes in the free space of growing stem tissues. Plant Physiol. 72: 326-331

Currier HB, Webster DH (1964) Callose Formation and Subsequent Disappearance: Studies in Ultrasound Stimulation. Plant Physiol. 39: 843-847

Dick PS, ap Rees T (1975) The Pathway of Sugar Transport in Roots of *Pisum sativum.* J. Exp. Bot. 26: 305-314

Ding B, Turgeon R, Parthasarathy MV (1992) Substructure of freeze-substituted plasmodesmata. Protoplasma 169: 28-41

Eastman P, Ann K, Peterson CA, Dengler NG (1988) Suberised Bundle Sheaths in Grasses *(Poaceae)* of Different Photosynthetic Types. II. Apoplastic Permeability. Protoplasma 142: 112-126

Eleftheriou EP (1990) Monocotyledons. Sieve Elements. In: Behnke H-D, Sjolund RD (eds) Comparative Structure, Induction and Development Springer, Berlin pp139-159. (not seen)

Eschrich W, Currier HB, Yamaguchi S, McNairn RB (1965) Der Eifluss vertärkter Callosebildung auf den Stofftransport in Siebröhren. Planta 65: 49-64 (not seen)

Eschrich W. (1980) Free space invertase, its possible role in phloem unloading. Ber. Deutsch. Bot. Ges. 93: 363-378 (not seen)

Evert RF, Eschrich W, Heyser W (1977) Distribution and Structure of the Plasmodesmata in Mesophyll and Bundle-sheath Cells of *Zea mays.* Planta 136: 77-89

Evert RF, Russin WA, Botha CEJ (1996) Distribution and frequency of plasmodesmata in relation to photoassimilate pathways and phloem loading in the barley leaf. Planta 198: 572-579

Farrar J, van der Schoot C, Drent P, van Bel AJE (1992) Symplastic transport of Lucifer Yellow in mature leaf blades of barley: potential mesophyll-to-sieve-tube transfer. New Phytol. 120: 191-196

Giaquinta RT, Lin W, Sadler NL, Franceschi VR (1983) Pathway of Phloem Unloading of Sucrose in Corn Roots. Plant Physiol. 72: 362-367

Glasziou KT (1960a) Accumulation and transformation of sugars in sugar cane stalks. Plant Physiol. 35: 895-901

Glasziou KT (1960b) Accumulation & transformation of sugars in stalks of sugar cane. Origin of glucose and fructose in the inner space. Plant Physiol. 36: 175-179

Glasziou KT, Gayler KR (1972) Storage of sugars in stalks of sugar cane. Bot. Rev. 38: 471-490

Goldner W, Thom M, Maretzki A (1991) Sucrose metabolism in sugarcane cell suspension cultures. Plant Sci. 73: 143-147

Gunning BES, Hughes JE (1976) Quantitative assessment of symplastic transport of prenectar into the trichomes of *Abutilon* nectaries. Aust. J. Plant Physiol. 3: 619-637

Hartt CE, Kortschak HP, Forbes AJ, Burr GO (1962) Translocation of C^{14} in Sugarcane. Plant Physiol. 38: 305-318

Hatch MD, Glasziou KT (1963a) Sugar accumulation cycle in sugar cane. II. Relationship of invertase activity to sugar content & growth rate in storage tissue of plants grown in controlled environments. Plant Physiol. 38: 344-348

Hatch MD, Glasziou KT (1963b) Direct Evidence for Translocation of Sucrose in Sugarcane Leaves and Stems. Plant Physiol. 39: 344-348

Hattersley PW, Watson L (1976) C_4 Grasses: An Anatomical Criterion for Distinguishing between NADP-Malic Enzyme Species and PCK or NAD-Malic Enzyme Species. Aust. J. Bot. 24: 297-308

Hattersley PW (1986) Variations in Photosynthetic Pathway. In: Soderstrom TR, Hilu KW, Campbell CS, Barkworth ME (eds) Grass Systematics and Evolution. Smithsonian Institution Press. Washington DC p59

Hawker JS (1965) The sugar content of cell walls and intercellular spaces in sugar-cane stems and its relation to sugar transport. Aust. J. Biol. Sci. 18: 959-969

Hayes PM, Patrick JW, Offler CE (1987) The Cellular Pathway of Radial Transfer of Photosynthates in Stems of *Phaseolus vulgaris* L.: Effects of Cellular Plasmolysis and p-Chloromercuribenzene Sulphonic Acid. Ann. Bot. 59: 635-642

Hitz WD, Scmitt MR, Card PJ, Giaquinta RT (1985) Transport and Metabolism of 1'-Fluorosucrose, a Sucrose Analog not Subject to Invertase Hydrolysis. Plant Physiol. 77: 291-295

Holdaway-Clarke TL, Walker AN, Hepler PK, Overall RL (2000) Physiological elevations in cytoplasmic free calcium by cold or ion injection result in transient closure of higher plant plasmodesmata. Planta 210: 329-335

Hong B, Ichida A, Wang Y, Gens JS, Pickard BG, Harper JF (1999) Identification of a Calmodulin-Regulated Ca^{2+}-ATPase in the Endoplasmic Reticulum. Plant Physiol. 119: 1165-1175

Hucket BI, Botha FC (1995) Stability and potential use of RAPD markers in a sugarcane genealogy. Euphytica 86: 117-125

Hughes JE, Gunning BES (1980) Glutaraldehyde-induced deposition of callose. Can. J. Bot. 58: 250-258

Jacobsen KR, Fisher DG, Maretzki A, Moore PH (1992) Developmental Changes in the Anatomy of the Sugarcane Stem in Relation to Phloem Unloading and Sucrose Storage. Bot. Acta. 105: 70-80

Kauss H (1987) Some aspects of calcium-dependent regulation in plant metabolism. Ann. Rev. Plant Physiol. 38: 47-72

Kempers R, Prior DAM, Oparka KJ, Knoblauch M, Van Bel AJE (1999) Integration of Controlled Intracellular Pressure Microinjection, Iontophoresis, and Membrane Potential Measurement. Plant Biol. 1: 61-67

Komor E, Thom M, Maretzki A (1981) The mechanism of sugar uptake by sugarcane suspension cells. Planta 153: 181-192

Komor E (1994) Regulation by Futile Cycles: The transport of Carbon and Nitrogen in Plants. In: Schultz E-D (ed) Flux Control in Biological Systems: from Enzymes to Populations and Ecosystems. Academic Press Limited. London pp153-201

Lucas WJ, Ding B, Van Der Schoot C (1993) Tansley Review No.58 Plasmodesmata and the supracellular nature of plants. New Phytol. 125: 435-476

Maretzki A, Thom M (1972) Membrane Transport of Sugars in Cell Suspensions of Sugarcane 1. Evidence for sites and specificity. Plant Physiol. 49: 177-182

Moore-Gordon CS, Cowen AK, Bertling I, Botha CEJ, Cross RHM (1998) Symplastic Solute Transport and Avocado Fruit Development: A Decline in Cytokinin / ABA Ratio is Related to Appearance of the Hass Small Fruit Variant. Plant Cell Physiol. 39: 1027-1038

Olesen P, Robards AW (1990) The neck region of plasmodesmata: general architecture and some functional aspects. In: Robards AW, Lucas WJ, Pitts JD, Jongsma HJ, Spray DC (eds) Parallels in Cell to Cell Junctions in Plants and Animals. Springer-Verlag, Berlin pp145-170

Oparka KJ, Prior DAM (1988) Movement of Lucifer Yellow CH in potato tuber storage tissues: A comparison of symplastic and apoplastic transport. Planta 176: 533-540

Oparka KJ, Prior DAM (1992) Direct evidence for pressure-generated closure of plasmodesmata. Plant J. 2: 741-750

Oparka KJ, Wright KM (1988) Influence of cell turgor on sucrose partitioning in potato tuber storage tissues. Planta 175: 520-526

Oparka KJ (1990) What is Phloem Unloading? Plant Physiol. 94: 393-396

Patrick JW (1990) Sieve element unloading: Cellular pathway, mechanism and control. Physiol. Plant. 78: 298-308

Patrick JW (1997) PHLOEM UNLOADING: Sieve Element Unloading and Post-Sieve Element Transport. Ann. Rev. Plant Physiol. Plant Molecular Biol. 48: 191-222

Pursglove JW (1979) Tropical Crops Monocotyledons. Longman Group Limited, London pp214-256

Radford JE, Vesk M, Overall RL (1997) Callose deposition at plasmodesmata. Protoplasma 201: 30-37

Robards AW, Lucas WJ (1990) Plasmodesmata. Ann. Rev. Plant Physiol. Plant Molecular Biol. 41: 369-419

Roberts AG, Santa Cruz S, Roberts IM, Prior DAM, Turgeon R (1997) Phloem Unloading in Sink Leaves of *Nicotiana bethamiana*: Comparison of a Fluorescent Solute with a Fluorescent Virus. Plant Cell 9: 1381-1396

Robinson-Beers K, Evert RF (1991) Ultrastructure of and plasmodesmatal frequency in mature leaves of sugarcane. Planta 184: 291-306

Schmalstig JG, Geiger DR (1985) Phloem Unloading in Developing Leaves of Sugar Beet 1. Evidence for pathway through the symplast. Plant Physiol. 76: 237-241

Schreiber L, Hartmann K, Skrabs M, Zeier J (1999) Apoplasmic barriers in roots: chemical composition of endodermal and hypodermal cell walls. J. Exp. Bot. 337: 1267-1280

Slack CR (1965) The physiology of sugar-cane III. Diurnal fluctuations in the activity of soluble invertase in elongating internodes. Aust. J. Biol. Sci. 18: 781-788

Smith MM, McCully ME (1978) A Critical Evaluation of the Specificity of Aniline Blue Induced Fluorescence. Protoplasma 95: 229-254

Spurr AR (1969) A low viscosity epoxy resin embedding medium for electron microscopy. J. Ultrastruct. Res. 26: 31-43

Thom, M, Maretzki A (1992) Evidence for Direct Uptake of Sucrose by Sugarcane Stalk Tissue. J. Plant Physiol. 139: 555-559

van Bel AJE, Hendriks JHM, Boon EJMC, Gamalai YV, van de Merwe APH. (1996) Different ratios of sucrose / raffinose-induced membrane depolarisations in the mesophyll of species with symplastic (*Catharanthus roseus*, *Ocimum basilicum*) apoplasmic (*Impatiens welleriana*, *Vicia faba*) minor-vein configurations. Planta 199: 185-193

van Bel AJE (1999) Evolution, polymorphology and multifunctionality of the phloem system. In: Edwards PJ, Fleischmann K, Endress P, Kollmann J, Newbery D, Conti E, Roy B, Schmid B (eds) Perspectives in Plant Ecology, Evolution and Systematics. Urban & Fischer Verlag, Zurich, Vol.2/2, pp 163-184

Veith R, Komor E (1993) Regulation of growth, sucrose storage and ion content in sugarcane cells, measured with suspension cells in continuous culture grown under nitrogen, phosphorus or carbon limitation. J. Plant Physiol. 142: 414-424

Waigmann E, Zambryski P (2000) Trichome Plasmodesmata: A Model System for Cell-to-cell Movement. In: Hallahan DL, Grey JC, Callow JA (eds) Advances in Botanical Research, incorporating Advances in Plant Pathology: Trichomes 31. Academic Press, pp261-283

Waigmann E, Turner A, Peart J, Roberts K, Zambryski P (1997) Ultrastructural analysis of leaf trichome plasmodesmata reveals major differences from mesophyll plasmodesmata. Planta 203: 75-84

Walsh KB, Sky RC, Brown SM (1996) Pathway of Sucrose Unloading from the Phloem in Sugarcane Stalk. In: Wilson JR, Hogarth DM, Campbell JA, Garside AL (eds) Research towards Efficient and Sustainable Production. Division of Tropical Crops and Pastures, Brisbane pp105-107

Welbaum GE, Meinzer FC (1990) Compartmentation of Solutes and Water in Developing Sugarcane Stalk Tissue. Plant Physiol. 93: 1147-1153

Welbaum GE, Meinzer FC, Grayson RL, Thornham KT (1992) Evidence for and Consequences of a Barrier to Solute Diffusion between the Apoplast and Vascular Bundles in Sugarcane Stalk Tissue. Aust. J. Plant Physiol. 19: 611-623

Whittaker A, Botha FC (1997) Carbon Partitioning during Sucrose Accumulation in Sugarcane Internodal Tissue. Plant Physiol. 115: 1651-1659

Williams L, Thom M, Maretzki A (1990) Characterisation of a proton translocating ATPase uptake in a tonoplast-enriched vesicle fraction from sugarcane. Physiol. Plant. 80: 169-176

Wolswinkel P (1985) Phloem unloading and turgor-sensitive transport: Factors involved in sink control of assimilate partitioning. Physiol. Plant. 65: 331-339

Wood RM, Patrick JW, Offler CE (1998) The Cellular Pathway of Short-distance Transfer of Photosynthates and Potassium in the Elongating Stem of *Phaseolus vulgaris* L. A Physiological Assessment. Ann. Bot. 82: 337-345

Wright KM, Oparka KJ (1997) Metabolic inhibiters induce symplasmic movement of solutes from the transport phloem of Arabidopsis roots. J. Exp. Bot. 315: 1807-1814

Wyse R (1979) Sucrose Uptake by Sugar Beet Tap Root Tissue. Plant. Physiol. 64: 837-841

Zimmermann HM, Steudle E (1998) Apoplastic transport across young maize roots: effect of the exodermis. Planta 206: 7-19